Developmental Biology
Genetics and Genomics

Coordinated *Tbx3 / Tbx5* transcriptional control of the adult ventricular conduction system

Reviewed Preprint
v1 • November 21, 2024
Not revised

Ozanna Burnicka-Turek, Katy A Trampel, Brigitte Laforest, Michael T Broman, Zoheb Khan, Eric Rytkin, Binjie Li, Ella Schaffer, Margaret Gadek, Kaitlyn M Shen, Igor R Efimov, Ivan P Moskowitz

Departments of Pediatrics, Pathology, and Human Genetics, University of Chicago, Chicago, USA • Departments of Biomedical Engineering, Northwestern University, Chicago, USA • Department of Medicine, Section of Cardiology, University of Chicago, Chicago, USA

eLife Assessment

The work presented is **important** for our understanding of the development of the cardiac conduction system and its regulation by T-box transcription factors. The conclusions are supported by **convincing** data. Overall this is an excellent study that advances our understanding of cardiac biology and has implications beyond the immediate field of study.

https://doi.org/10.7554/eLife.102027.1.sa3

Abstract

The cardiac conduction system (CCS) orchestrates the electrical impulses that enable coordinated contraction of the cardiac chambers. The T-box transcription factors *TBX3* and *TBX5* are required for cardiac conduction system development and associated with overlapping and distinct human cardiac conduction system diseases. We evaluated the coordinated role of *Tbx3* and *Tbx5* in the murine ventricular conduction system (VCS). We engineered a compound *Tbx3:Tbx5* conditional knockout allele for both genes located in *cis* on mouse chromosome 5. Conditional deletion of both T-box transcriptional factors in the ventricular conduction system, using the VCS-specific *Mink:Cre,* caused loss of VCS function and molecular identity. Combined *Tbx3* and *Tbx5* deficiency in the adult VCS led to conduction defects, including prolonged PR and QRS intervals and elevated susceptibility to ventricular tachycardia. These electrophysiologic defects occurred prior to detectable alterations in cardiac contractility or histologic morphology, indicative of a primary conduction system defect. *Tbx3:Tbx5* double knockout VCS cardiomyocytes revealed a transcriptional shift towards non-CCS-specialized working myocardium, suggesting reprogramming of their cellular identity. Furthermore, optical mapping revealed a loss of VCS-specific conduction system propagation. Collectively, these findings indicate that *Tbx3* and *Tbx5* coordinate to control VCS molecular fate and function, with implications for understanding cardiac conduction disorders in humans.

Introduction

The cardiac conduction system (CCS) constitutes a highly specialized network of cardiomyocytes that initiate and propagate the electrical impulses required for synchronized contractions of the heart. In the mature mammalian heart, the functional components of the CCS can be broadly divided into the slowly propagating atrial nodes (~ 5cm/sec), containing the sinoatrial node (SAN) and atrioventricular node (AVN), and the rapidly propagating ventricular conduction system (VCS) (~ 200cm/sec), including the AV (His) bundle (AVB) and the right and left bundle branches (BBs). The VCS is responsible for rapid propagation of the electrical impulse from the AVN to the ventricular apex to enable synchronous ventricular contraction and effective ejection of blood from the ventricles (1–3). Defects of CCS can occur in normally formed hearts as well as in patients with structural congenital heart disease and are a major source of morbidity and mortality (1, 3–6). The VCS specifically has been recognized as a substrate for life-threatening ventricular arrhythmias, including bundle branch reentry tachycardia, idiopathic fascicular tachycardia, short-coupled torsade de pointes, and ventricular fibrillation (1, 6–9). Despite the severe clinical consequences of CCS disorders, the molecular mechanisms that establish and maintain regional functionality of the mature CCS domains require further study.

Human genetic studies have identified numerous loci associated with adult human CCS function, including the developmentally important factors *Tbx3* and *Tbx5* (reviewed in 1, 10). *Tbx3* and *Tbx5* play crucial roles in adult CCS development and function (1, 3, 11–20). *Tbx5* encodes a T-box transcriptional activator required for structural and conduction system cardiac development (3, 12, 20, 21). Dominant mutations in human *TBX5* cause Holt-Oram syndrome (HOS, OMIM:142900), an autosomal dominant disorder characterized by upper limb malformations, congenital heart defects and CCS abnormalities (22–24). The cardiac phenotype of HOS, including atrioventricular conduction delay, has been recapitulated in the *Tbx5* heterozygous mice (20). Moreover, VCS-specific *Tbx5* knockout caused slowed VCS function and ventricular tachycardia resulting in sudden death in mice (1), emphasizing the importance of *Tbx5* in VCS conduction. *Tbx5* is strongly expressed in the atria and VCS (1, 3, 12, 17), and directly regulates several targets required for VCS function (3, 20, 25), including *Gja5 (Cx40)* (20) and *Scn5a (Nav1.5)* (1). *Tbx3* encodes a T-box transcriptional repressor which is critical for cardiac development (17, 26). Dominant mutations in human *TBX3* cause Ulnar-Mammary syndrome (OMIM:181450), a developmental disorder (27, 28), that includes functional conduction system defects (29). In the heart, *Tbx3* is specifically expressed within CCS (17, 30), and its deficiency below critical level leads to lethal arrhythmias (26). Furthermore, *Tbx3* is required for the molecular identity but not the function of the VCS (17). In contrast, *Tbx3* in SAN and AVN is required for their proper function (30), emphasizing its critical role in maintaining proper cardiac rhythm.

A model for regional CCS patterning suggests that the adult CCS is patterned entirely as a slow conduction system ground state by *Tbx3* with a T-box-dependent, physiologically dominant fast conduction system network driven specifically in the VCS by *Tbx5* (11). Adult VCS-specific removal of TBX5 or overexpression of TBX3 re-patterned the fast VCS into a slow nodal-like system, indicating that the *Tbx3/Tbx5* ratio determines nodal versus VCS function (11). However, a comprehensive assessment of the coordinated requirements for *Tbx3* and *Tbx5* has been hindered by the inability to achieve their compound deletion due to their genomic proximity. *Tbx3* and *Tbx5* are situated in *cis* within 0.6 Mb on chromosome 5 in mice, rendering their simultaneous deletion unattainable with the available single allele conditional alleles. To investigate the consequences of *Tbx3* and *Tbx5* compound removal from the VCS, we generated a novel compound *Tbx3:Tbx5* double conditional allele. We found that VCS-specific genetic removal of both TBX3 and TBX5 transformed fast-conducting, adult VCS into working myocardium-like

cardiomyocytes, re-patterning them from conduction to non-conduction myocytes. These results demonstrated the coordinated requirements of both *Tbx3* and *Tbx5* for maintained specification of the mature ventricular conduction system.

Results

We generated a novel *Tbx3:Tbx5* double-floxed allele to enable the simultaneous conditional deletion of *Tbx3* and *Tbx5* genes specifically from the adult VCS. *Tbx3* and *Tbx5* reside in *cis* on mouse chromosome 5 (*Tbx3* mm39 chr5:119808734-119822789; *Tbx5* mm39 chr5:119970733-120023284). Therefore, to generate a double-conditional knockout, we targeted *Tbx5* in the background of a previously validated *Tbx3* floxed allele (26) using the CRISPR-Cas9 system (31, 32) (**Figure 1A**). We engineered a *Tbx5* floxed allele mirroring a previously published allele (20). This design enabled us to utilize the previously published individual *Tbx3* floxed allele (26) and individual *Tbx5* floxed allele (20) to serve as controls (**Figure 1A** and Supplementary Figure 1 and 2).

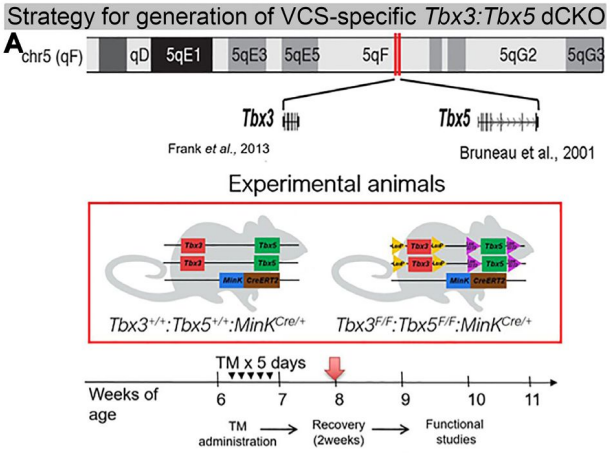
Strategy for generation of VCS-specific Tbx3:Tbx5 dCKO
A
chr5 (qF)
qD
5qE1
5qE3
5qE5
5qF
5qG2
5qG3
Tbx3
Tbx5
Frank et al., 2013
Bruneau et al., 2001
Experimental animals
Tbx3+/+:Tbx5+/+:MinKCre/+
Tbx3F/F:Tbx5F/F:MinKCre/+
TM x 5 days
Weeks of age
6
7
8
9
10
11
TM administration
Recovery (2weeks)
Functional studies

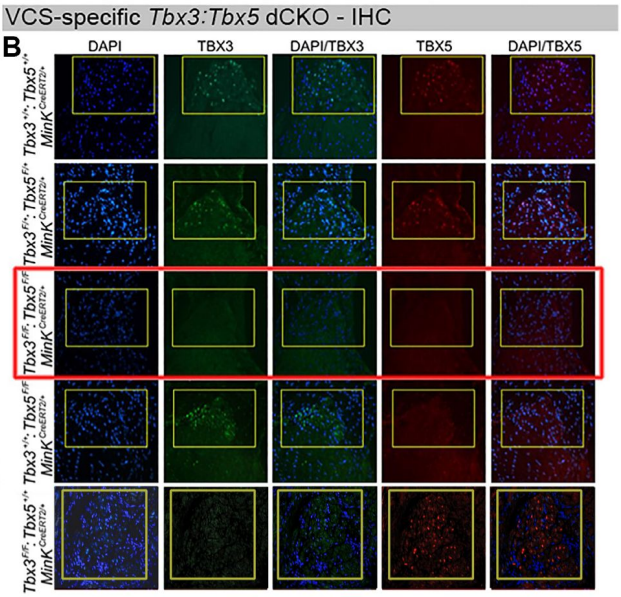
VCS-specific Tbx3:Tbx5 dCKO - IHC
B
DAPI
TBX3
DAPI/TBX3
TBX5
DAPI/TBX5

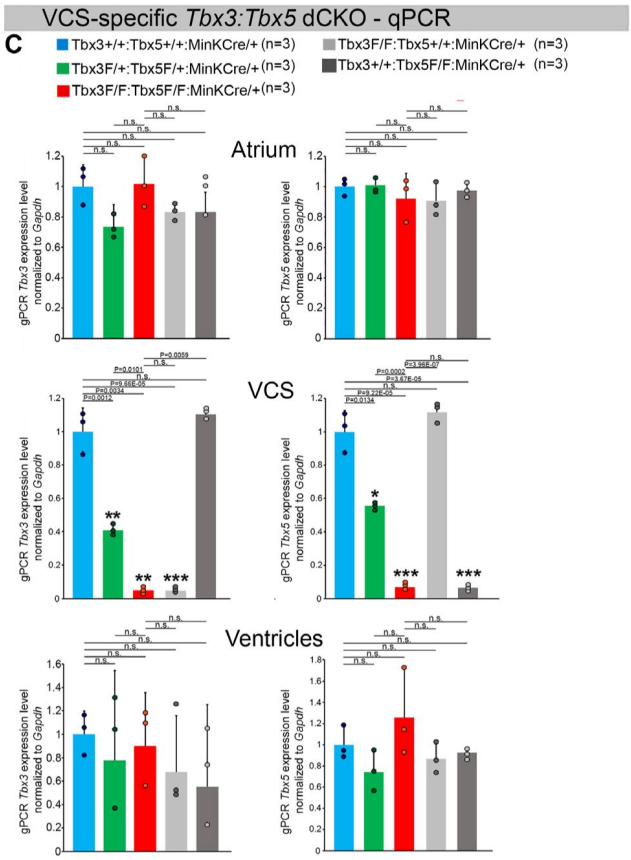
VCS-specific Tbx3:Tbx5 dCKO - qPCR
C
Tbx3+/+:Tbx5+/+:MinKCre/+ (n=3)
Tbx3F/+:Tbx5F/+:MinKCre/+ (n=3)
Tbx3F/F:Tbx5F/F:MinKCre/+(n=3)
Tbx3F/F:Tbx5+/+:MinKCre/+ (n=3)
Tbx3+/+:Tbx5F/F:MinKCre/+ (n=3)
Atrium
VCS
Ventricles
gPCR Tbx3 expression level normalized to Gapdh
gPCR Tbx5 expression level normalized to Gapdh

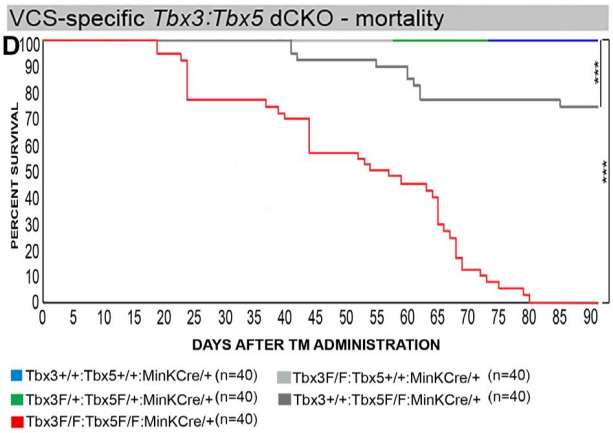
VCS-specific Tbx3:Tbx5 dCKO - mortality
D
PERCENT SURVIVAL
DAYS AFTER TM ADMINISTRATION
Tbx3+/+:Tbx5+/+:MinKCre/+ (n=40)
Tbx3F/+:Tbx5F/+:MinKCre/+ (n=40)
Tbx3F/F:Tbx5F/F:MinKCre/+(n=40)
Tbx3F/F:Tbx5+/+:MinKCre/+ (n=40)
Tbx3+/+:Tbx5F/F:MinKCre/+ (n=40)

Figure 1.

Generation of VCS-specific *Tbx3:Tbx5* double-conditional knockout mice.

(A) Strategy to generate VCS-specific Tbx3*:Tbx5* double-conditional knockout mouse line. A new *Tbx3:Tbx5* double-conditional knockout mouse line (*Tbx3*$^{fl/fl}$;*Tbx5*$^{fl/fl}$) was generated using the CRISPR-Cas9 system (31, 32) which allowed for the targeting of*Tbx5* in the background of the previously validated *Tbx3* floxed allele (26). A newly engineered *Tbx5* floxed allele has been developed to mirror a previously published allele (20). This design has enabled the utilization of the previously published individual *Tbx3* floxed allele (26) and individual *Tbx5* floxed allele (20) as controls. To conditionally delete *Tbx3* and *Tbx5* genes specifically from the adult VCS and generate the experimental animals, the *Tbx3:Tbx5* double-floxed mouse line (*Tbx3*$^{fl/fl}$;*Tbx5*$^{fl/fl}$) was combined with a VCS-specific tamoxifen inducible *Cre* transgenic mouse line (MinK^{CreERT2} [Tg(RP23-276I20-MinkCreERT2) (8). All allelic combinations were generated and evaluated as littermates in a mixed genetic background. The experimental mice employed in all studies were administered tamoxifen at 6 weeks of age and subsequently evaluated at 8 weeks of age (2 weeks post-tamoxifen administration). **(B, C)** The loss of *Tbx3* and *Tbx5* expression, on both the protein and mRNA levels, assessed by immunohistochemistry **(B)** and qPCR **(C)**, respectively, was observed in the VCS of adult *Tbx3:Tbx5* double-conditional mutant mice (*Tbx3*$^{fl/fl}$;*Tbx5*$^{fl/fl}$;*R26*$^{EYFP/+}$;*MinK*$^{CreERT2/+}$), but not in their littermate controls (*Tbx3*$^{+/+}$;*Tbx5*$^{+/+}$;*R26*$^{EYFP/+}$;*MinK*$^{CreERT2/+}$) **(B and C)**. **(C)** QPCR analysis showed a partial loss of *Tbx3* and *Tbx5* expression in the adult VCS of *Tbx3:Tbx5* double-conditional heterozygous mice (*Tbx3*$^{fl/+}$;*Tbx5*$^{fl/+}$;*R26*$^{EYFP/+}$; *MinK*$^{CreERT2/+}$) compared to their littermate controls (*Tbx3*$^{+/+}$;*Tbx5*$^{+/+}$;*R26*$^{EYFP/+}$; *MinK*$^{CreERT2/+}$). Additionally, qPCR analysis confirmed the specificity of the *Tbx3:Tbx5* double knockout for the VCS by assessing *Tbx3* and Tbx5 expression levels in the atria and ventricles of tamoxifen-treated experimental mice. Consistent with the VCS selectivity of Cre activity in the MinKCreERT2 mice (8), *Tbx3* and *Tbx5* expression remained similar in the atrial and ventricular myocardium across all allelic combinations, including *Tbx3:Tbx5* double-conditional knockout mice (*Tbx3*$^{fl/fl}$;*Tbx5*$^{fl/fl}$;*R26*$^{EYFP/+}$;*MinK*$^{CreERT2/+}$). **(D)** Conducted longitudinal studies revealed a significantly increased mortality rate in VCS-specific *Tbx3:Tbx5*-deficient mice compared to their littermate controls (***$P < 0.0001$, log-rank test), suggesting a requirement for both *Tbx3* and *Tbx5* in the mature VCS. All allelic combinations of experimental and control mice (n=40 biological replicates/genotype) were followed longitudinally after tamoxifen administration at 6 weeks of age. *Tbx3:Tbx5* double-conditional knockout mice began to die suddenly at 3 to 4 weeks post-tamoxifen administration. Within the 3 months post-tamoxifen administration, all tamoxifen-treated *Tbx3*$^{fl/fl}$;*Tbx5*$^{fl/fl}$;*R26*$^{EYFP/+}$;*MinK*$^{CreERT2/+}$ mice had died suddenly (n=40) without previous signs of illness. In contrast, no mortality was observed among the tamoxifen-treated *Tbx3*$^{+/+}$;*Tbx5*$^{+/+}$;*R26*$^{EYFP/+}$;*MinK*$^{CreERT2/+}$ *and* *Tbx3*$^{fl/+}$;*Tbx5*$^{fl/+}$;*R26*$^{EYFP/+}$;*MinK*$^{CreERT2/+}$ littermates (each cohort n=40) during this period. TBX3 and TBX5 protein expression was evaluated by immunohistochemistry (green and red signals, respectively) on serial sections from hearts of all allelic combinations (n=3 biological replicates/genotype). Nuclei were stained with DAPI (blue signal). IHC original magnification: 40x. QPCR data are presented as mean±SD normalized to *Gapdh* and relative to *Tbx3*$^{+/+}$;*Tbx5*$^{+/+}$;*R26*$^{EYFP/+}$;*MinK*$^{CreERT2/+}$ mice (set as 1). Welch *t* test: *P<0.05; **P<0.005; *** P<0.001; n=3 biological replicates/genotype (VCS cardiomyocytes pooled from 30 mice per each biological replicate); multiple testing correction using Benjamini & Hochberg procedure; *false discovery rate ≤0.05.

We assessed the impact of removing *Tbx3* and *Tbx5* from the mature VCS by combining the *Tbx3:Tbx5* double-floxed mouse line (*Tbx3*$^{fl/fl}$;*Tbx5*$^{fl/fl}$) with a VCS-specific tamoxifen (TM) inducible *Cre* transgenic mouse line (MinK^{CreERT2} [Tg(RP23-276I20-MinkCreERT2) (**Figure 1A**) (8). Individual *Tbx3* floxed and *Tbx5* floxed mouse lines combined with *Mink*^{CreERT2} transgenic mouse lines (*Tbx3*$^{fl/fl}$;*Tbx5*$^{+/+}$; *R26*$^{EYFP/+}$;*MinK*$^{CreERT2/+}$ and *Tbx3*$^{+/+}$;*Tbx5*$^{fl/fl}$;*R26*$^{EYFP/+}$;*MinK*$^{CreERT2/+}$, respectively), were generated as controls, and all allelic combinations were evaluated in a mixed genetic background. We compared VCS-specific *Tbx3:Tbx5* double-conditional mutants (*Tbx3*$^{fl/fl}$;*Tbx5*$^{fl/fl}$;*R26*$^{EYFP/+}$;*MinK*$^{CreERT2/+}$) with control littermates (*Tbx3*$^{+/+}$;*Tbx5*$^{+/+}$; *R26*$^{EYFP/+}$;*MinK*$^{CreERT2/+}$) and VCS-specific *Tbx3:Tbx5* double-conditional heterozygous littermates (*Tbx3*$^{fl/+}$;*Tbx5*$^{fl/+}$;*R26*$^{EYFP/+}$;*MinK*$^{CreERT2/+}$). Additionally, we validated the newly created *Tbx5* floxed allele demonstrating that it is efficiently converted to the

Tbx5 null allele through *Cre* recombinase, causing a phenotype consistent with that observed from conversion of the previously published *Tbx5* floxed allele (1, 20) (Supplementary Figure 1 and 2, Supplementary Material section).

We assessed experimental mice at 8-9 weeks of age following tamoxifen administration at 6 weeks of age (**Figure 1A**, Methods section). We observed loss of both *Tbx3* and *Tbx5* expression, on both the mRNA and protein levels, in the VCS of adult *Tbx3:Tbx5* double-conditional mutant mice ($Tbx3^{fl/fl};Tbx5^{fl/fl};R26^{EYFP/+};MinK^{CreERT2/+}$) but not in their littermate controls ($Tbx3^{+/+};Tbx5^{+/+};R26^{EYFP/+};MinK^{CreERT2/+}$) (**Figure 1B** and **C**). Partial loss of *Tbx3* and *Tbx5* expression in the adult VCS of *Tbx3:Tbx5* double-conditional heterozygous mice ($Tbx3^{fl/+};Tbx5^{fl/+};R26^{EYFP/+};MinK^{CreERT2/+}$) was observed compared to littermate controls ($Tbx3^{+/+};Tbx5^{+/+};R26^{EYFP/+};MinK^{CreERT2/+}$) (**Figure 1C**). We confirmed the specificity of the *Tbx3:Tbx5* double knockout for the VCS by assessing *Tbx3* and *Tbx5* expression levels in the atria and ventricles of tamoxifen-treated experimental mice. Consistent with the VCS selectivity of *Cre* activity in the $MinK^{CreERT2}$ mice (8), *Tbx3* and *Tbx5* expression remained similar in the atrial and ventricular myocardium of all allelic combinations, including *Tbx3:Tbx5* double-conditional knockout mice ($Tbx3^{fl/fl};Tbx5^{fl/fl};R26^{EYFP/+};MinK^{CreERT2/+}$) (**Figure 1C**).

Tbx3:Tbx5 double-conditional knockout mice ($Tbx3^{fl/fl};Tbx5^{fl/fl};R26^{EYFP/+};MinK^{CreERT2/+}$) appeared morphologically and functionally normal and indistinguishable from control littermates ($Tbx3^{+/+};Tbx5^{+/+};R26^{EYFP/+};MinK^{CreERT2/+}$) at 2 weeks post-tamoxifen. However, longitudinal analysis demonstrated sudden death of VCS-specific double knockout mice beginning 3 weeks post-tamoxifen administration (**Figure 1D**). Within the 3 months post-tamoxifen administration, all tamoxifen-treated $Tbx3^{fl/fl};Tbx5^{fl/fl};R26^{EYFP/+};MinK^{CreERT2/+}$ mice had died suddenly (n=40). In contrast, no mortality was observed among the tamoxifen-treated $Tbx3^{+/+};Tbx5^{+/+};R26^{EYFP/+};MinK^{CreERT2/+}$ or $Tbx3^{fl/+};Tbx5^{fl/+};R26^{EYFP/+};MinK^{CreERT2/+}$ littermates (each cohort n=40) during this period (*Tbx3:Tbx5* double-conditional knockout mice vs control mice P<0.0001; *Tbx3:Tbx5* double-conditional knockout mice vs *Tbx3:Tbx5* double-conditional heterozygous mice P<0.0001, log-rank test; **Figure 1D**). These results revealed that double deletion of *Tbx3* and *Tbx5* from the adult VCS causes lethality beginning at 3 weeks post-tamoxifen.

The onset of mortality observed in VCS-specific *Tbx3:Tbx5*-deficient mice starting at 3 weeks post-tamoxifen prompted us to investigate the electrophysiologic consequences of VCS-specific *Tbx3:Tbx5* double-knockout at 2-3 weeks post-tamoxifen, prior to the onset of lethality (**Figure 2**). VCS-specific *Tbx3:Tbx5*-deficiency caused profound conduction slowing in $Tbx3^{fl/fl};Tbx5^{fl/fl};R26^{EYFP/+};MinK^{CreERT2/+}$ mice by ambulatory telemetry ECG analysis compared to *Tbx3:Tbx5* double-conditional heterozygous mice ($Tbx3^{fl/+};Tbx5^{fl/+};R26^{EYFP/+};MinK^{CreERT2/+}$) and littermate controls ($Tbx3^{+/+};Tbx5^{+/+};R26^{EYFP/+};MinK^{CreERT2/+}$) (**Figure 2A-F**). Specifically, the PR interval, representing the period between atrial and ventricular depolarization, and the QRS duration, indicating the length of ventricular depolarization and early repolarization in mice, were both significantly prolonged (**Figure 2A, B**, and **D**; PR: *Tbx3:Tbx5* double-conditional knockout mice vs control mice P<0.05, n=5, Welch *t* test; QRS: *Tbx3:Tbx5* double-conditional knockout mice vs control mice P<0.05, n=5, Welch *t* test). Removal of both *Tbx3* and *Tbx5* from the adult VCS resulted in increased episodes of spontaneous ventricular tachycardia (VT). Ambulatory studies revealed episodes of spontaneous VT in 4 out of 7 $Tbx3^{fl/fl};Tbx5^{fl/fl};R26^{EYFP/+};MinK^{CreERT2/+}$ mice, in contrast to none observed in 7 littermate controls (**Figure 2G**, P<0.05, n=7, Welch *t* test). Furthermore, *Tbx3:Tbx5* double-conditional knockout mice ($Tbx3^{fl/fl};Tbx5^{fl/fl};R26^{EYFP/+};MinK^{CreERT2/+}$) showed significantly increased susceptibility to ventricular tachycardia following burst stimulation in invasive electrophysiology (EP) studies (3 of 3 $Tbx3^{fl/fl};Tbx5^{fl/fl};R26^{EYFP/+};MinK^{CreERT2/+}$ mice versus 0 of 7 littermate controls; (**Figure 2H**, P<0.05, Welch *t* test). In contrast, VCS-specific *Tbx3:Tbx5* double-conditional heterozygous mice (n=7) showed neither conduction nor electrophysiological defects (**Figure 2**). Consistent with the use of a VCS-specific *Cre* (*Mink-Cre*), no changes in the refractory/recovery periods of atrium, ventricle, or nodes (atrial effective refractory period, ventricular effective refractory period,

atrioventricular nodal effective refractory period, or sinus node recovery time) were detected by intracardiac electrophysiology conducted on experimental and control mice (**Figure 2I**, $P<0.05$, Welch *t* test).

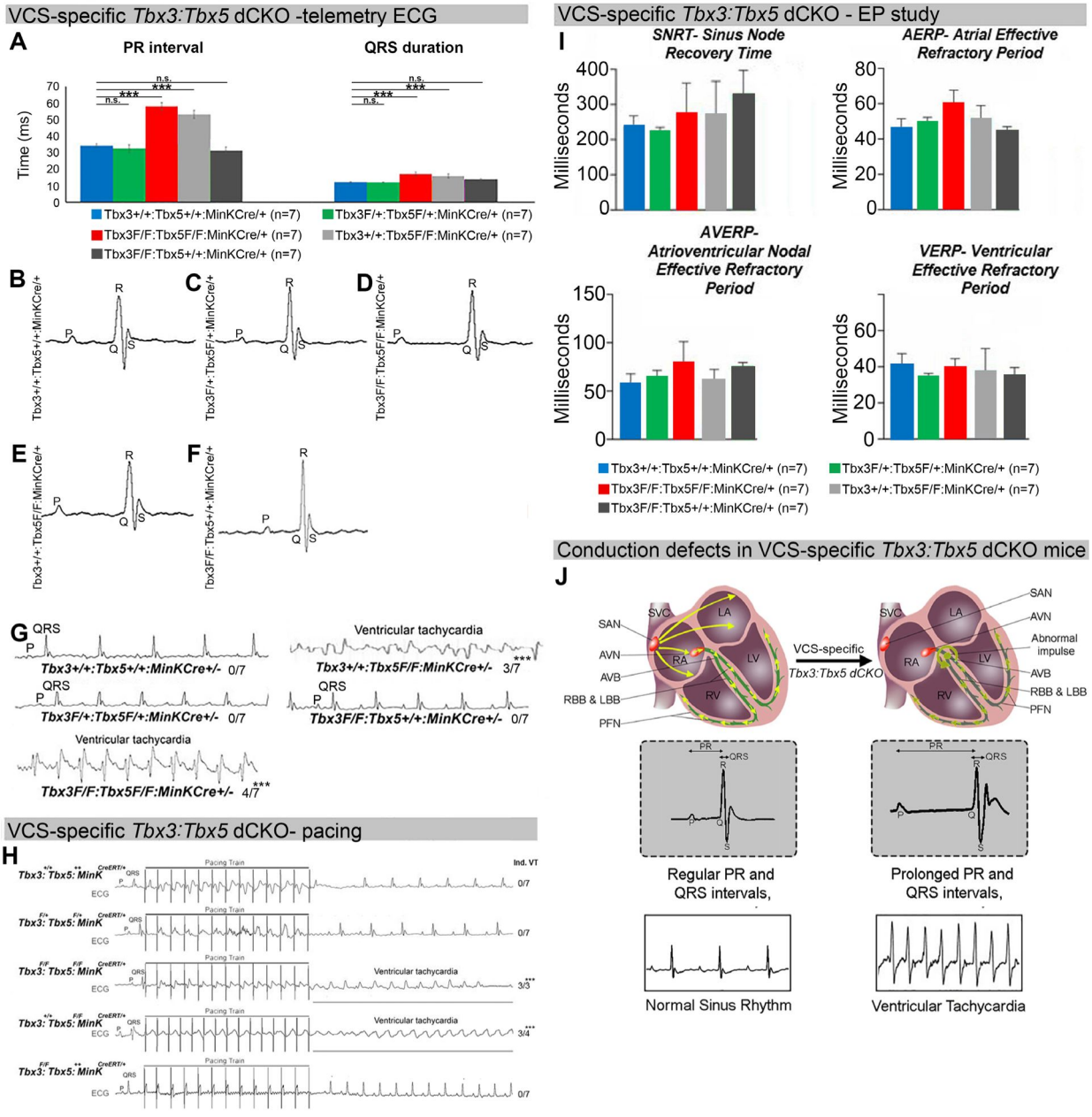
VCS-specific Tbx3:Tbx5 dCKO -telemetry ECG
A
PR interval
QRS duration
Time (ms)
Tbx3+/+:Tbx5+/+:MinKCre/+ (n=7)
Tbx3F/+:Tbx5F/+:MinKCre/+ (n=7)
Tbx3F/F:Tbx5F/F:MinKCre/+ (n=7)
Tbx3+/+:Tbx5F/F:MinKCre/+ (n=7)
Tbx3F/F:Tbx5+/+:MinKCre/+ (n=7)
B
C
D
E
F
G
QRS
Ventricular tachycardia
Tbx3+/+:Tbx5+/+:MinKCre+/- 0/7
Tbx3+/+:Tbx5F/F:MinKCre+/- 3/7
Tbx3F/+:Tbx5F/+:MinKCre+/- 0/7
Tbx3F/F:Tbx5+/+:MinKCre+/- 0/7
Tbx3F/F:Tbx5F/F:MinKCre+/- 4/7
VCS-specific Tbx3:Tbx5 dCKO- pacing
H
Pacing Train
Ind. VT
ECG
Ventricular tachycardia
VCS-specific Tbx3:Tbx5 dCKO - EP study
I
SNRT- Sinus Node Recovery Time
AERP- Atrial Effective Refractory Period
AVERP- Atrioventricular Nodal Effective Refractory Period
VERP- Ventricular Effective Refractory Period
Milliseconds
Tbx3+/+:Tbx5+/+:MinKCre/+ (n=7)
Tbx3F/+:Tbx5F/+:MinKCre/+ (n=7)
Tbx3F/F:Tbx5F/F:MinKCre/+ (n=7)
Tbx3+/+:Tbx5F/F:MinKCre/+ (n=7)
Tbx3F/F:Tbx5+/+:MinKCre/+ (n=7)
Conduction defects in VCS-specific Tbx3:Tbx5 dCKO mice
J
SAN
AVN
AVB
RBB & LBB
PFN
SVC
LA
RA
LV
RV
VCS-specific
Tbx3:Tbx5 dCKO
Abnormal impulse
PR
QRS
Regular PR and QRS intervals,
Prolonged PR and QRS intervals,
Normal Sinus Rhythm
Ventricular Tachycardia

Figure 2.

Arrhythmias and conduction abnormalities in mice with VCS-specific *Tbx3:Tbx5* double-conditional knockout.

(A-F) VCS-specific *Tbx3:Tbx5* double-conditional knockout causes significant VCS conduction slowing in adult $Tbx3^{fl/fl}$;$Tbx5^{fl/fl}$;$R26^{EYFP/+}$;$MinK^{CreERT2/+}$ mice. **(A)** PR **(left graph)** and QRS **(right graph)** intervals calculated from ambulatory telemetry ECG recordings in (B-F). *Tbx3:Tbx5* double-conditional adult mice ($Tbx3^{fl/fl}$;$Tbx5^{fl/fl}$;$R26^{EYFP/+}$;$MinK^{CreERT2/+}$) displayed significant PR and QRS intervals prolongation compared to littermate controls ($Tbx3^{+/+}$;$Tbx5^{+/+}$;$R26^{EYFP/+}$;$MinK^{CreERT2/+}$) **(A left and right graphs, respectively)**. Data are presented as mean±SD. Welch t test: *P<0.05; n=7 biological replicates/genotype, multiple testing correction using Benjamini & Hochberg procedure; *false discovery rate ≤0.05. **(B-F)** Representative ambulatory telemetry ECG of $Tbx3^{+/+}$;$Tbx5^{+/+}$; $R26^{EYFP/+}$;$MinK^{CreERT2/+}$ **(B),** $Tbx3^{fl/+}$;$Tbx5^{fl/+}$;$R26^{EYFP/+}$;$MinK^{CreERT2/+}$ **(C),** $Tbx3^{fl/fl}$;$Tbx5^{fl/fl}$; $R26^{EYFP/+}$;$MinK^{CreERT2/+}$ **(D),** $Tbx3^{fl/fl}$;$Tbx5^{+/+}$;$R26^{EYFP/+}$;$MinK^{CreERT2/+}$ **(E),** $Tbx3^{+/+}$;$Tbx5^{fl/fl}$; $R26^{EYFP/+}$;$MinK^{CreERT2/+}$ **(F)** mice. **(G)** Simultaneous genetic removal of *Tbx3* and *Tbx5* from the adult VCS resulted in significantly increased episodes of spontaneous ventricular tachycardia. Episodes of spontaneous ventricular tachycardia were observed in 4 of 7 $Tbx3^{fl/fl}$;$Tbx5^{fl/fl}$;$R26^{EYFP/+}$;$MinK^{CreERT2/+}$ *mice versus* 0 of 7 littermate controls ($Tbx3^{+/+}$;$Tbx5^{+/+}$;$R26^{EYFP/+}$;$MinK^{CreERT2/+}$) in ambulatory studies. Welch *t* test: *P<0.05; n=7 biological replicates/genotype; multiple testing correction using Benjamini & Hochberg procedure; *false discovery rate ≤0.05. **(H)** *Tbx3:Tbx5* double-conditional knockout mice ($Tbx3^{fl/fl}$;$Tbx5^{fl/fl}$;$R26^{EYFP/+}$;$MinK^{CreERT2/+}$) showed significantly increased susceptibility to ventricular tachycardia following burst stimulation in invasive electrophysiology studies (3 of 3 $Tbx3^{fl/fl}$;$Tbx5^{fl/fl}$;$MinK^{CreERT2/+}$ mice versus 0 of 7 control $Tbx3^{+/+}$;$Tbx5^{+/+}$;$R26^{EYFP/+}$;$MinK^{CreERT2/+}$.mice. Fisher's exact test: *P<0.05; n=7 biological replicates/genotype). **(I)** Intracardiac electrophysiology detected no significant changes in SNRT, AERP, AVERP, and VERP recorded from experimental and control animals (Welch *t* test: *P<0.05; n=7 biological replicates/genotype; multiple testing correction using Benjamini & Hochberg procedure; *false discovery rate ≤0.05). **(J)** Graphical summary of conduction defects observed in adult, VCS-specific *Tbx3:Tbx5*-deficient mice. Simultaneous genetic deletion of *Tbx3* and *Tbx5* from the mature VCS results in conduction slowing, prolonged PR and QRS intervals, as well as ventricular tachycardia.

To distinguish a primary conduction system abnormality from a secondary conduction abnormality resulting from cardiac dysfunction or remodeling, we evaluated cardiac form and function at the time of arrhythmia assessment, 2-3 weeks post-tamoxifen treatment (**Figure 3**). Transthoracic echocardiography revealed no significant differences in left ventricular ejection fraction (LVEF) and fractional shortening (FS) between VCS-specific *Tbx3:Tbx5*-deficient ($Tbx3^{fl/fl}$;$Tbx5^{fl/fl}$;$R26^{EYFP/+}$;$MinK^{CreERT2/+}$) and control ($Tbx3^{+/+}$;$Tbx5^{+/+}$;$R26^{EYFP/+}$;$MinK^{CreERT2/+}$) mice *(LVEF: Tbx3:Tbx5* double-conditional knockout mice vs control mice P<0.05, n=7, Welch *t* test; and FS: *Tbx3:Tbx5* double-conditional knockout mice vs control mice P>0.05, n=7, Welch *t* test; **Figure 3A**, **3B** and **3D**). Histological examination of all four-chambers demonstrated no discernible differences between VCS-specific *Tbx3:Tbx5* double-knockout ($Tbx3^{fl/fl}$;$Tbx5^{fl/fl}$;$R26^{EYFP/+}$; $MinK^{CreERT2/+}$) and control ($Tbx3^{+/+}$;$Tbx5^{+/+}$;$R26^{EYFP/+}$; $MinK^{CreERT2/+}$) mice. Ventricular muscle appeared normal without hypertrophy or myofibrillar disarray and no fibrosis was present (**Figure 3G** and **3I**). QRT-PCR analysis for fibrosis genes *Col1a1* (33–35) and *Postn* (35–38) further confirmed no fibrosis in VCS of *Tbx3:Tbx5*-deficient mice (**Figure 3L**). No contractile dysfunction, histological abnormalities, or increased expression of fibrosis genes were observed in VCS-specific *Tbx3:Tbx5* double-conditional heterozygous mice ($Tbx3^{fl/+}$;$Tbx5^{fl/+}$;$R26^{EYFP/+}$; $MinK^{CreERT2/+}$) (**Figure 3A**, **3C**, **3H**, and **3L**). Taken together, these data indicate that the conduction defect and ventricular tachycardia observed in mice with VCS-specific *Tbx3:Tbx5* deletion (**Figure 2**) occur prior to the onset of left ventricular dysfunction or evidence of remodeling (**Figure 3**), implying a primary origin.

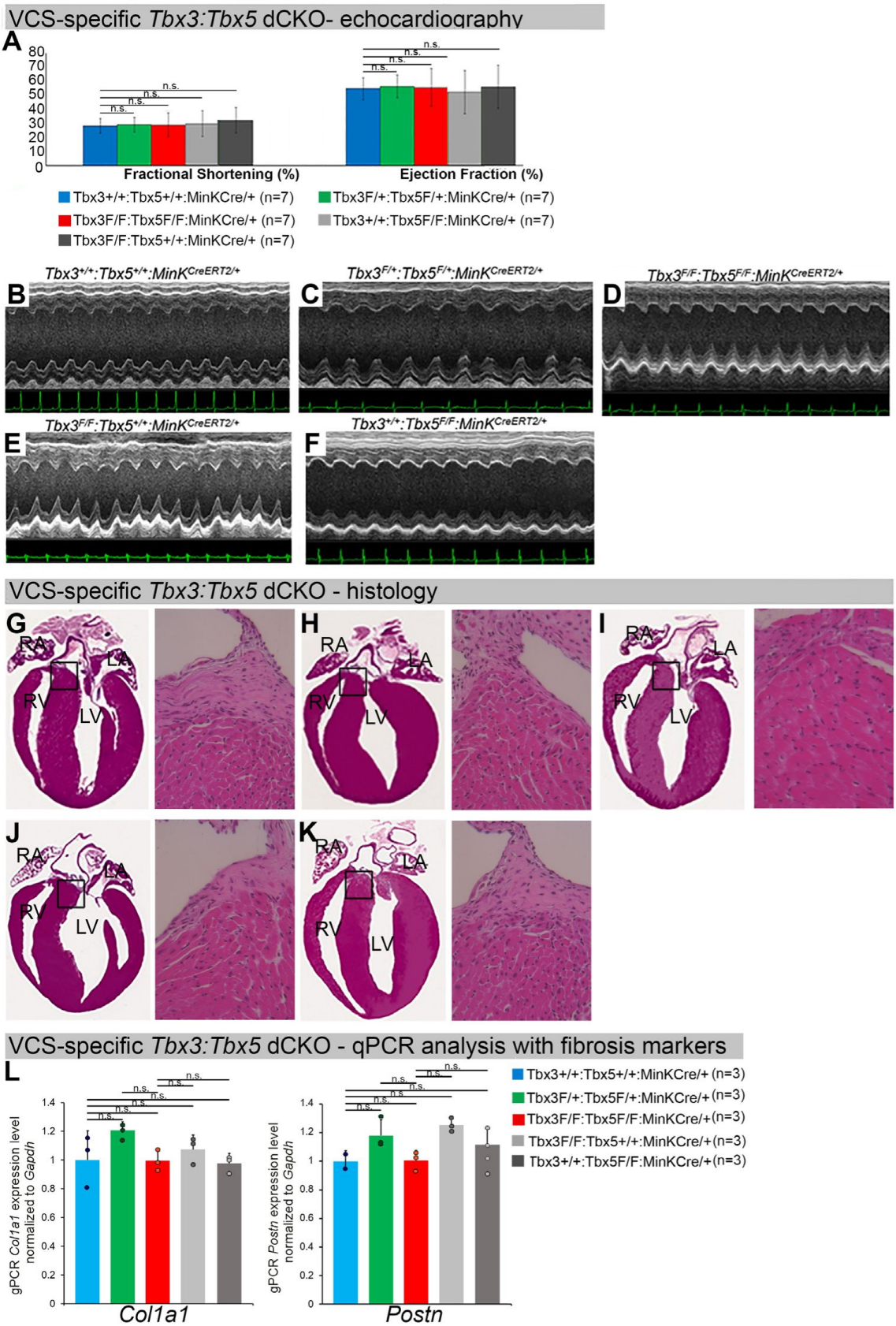
VCS-specific Tbx3:Tbx5 dCKO- echocardiography
A
Fractional Shortening (%)
Ejection Fraction (%)
n.s.
Tbx3+/+:Tbx5+/+:MinKCre/+ (n=7)
Tbx3F/+:Tbx5F/+:MinKCre/+ (n=7)
Tbx3F/F:Tbx5F/F:MinKCre/+ (n=7)
Tbx3+/+:Tbx5F/F:MinKCre/+ (n=7)
Tbx3F/F:Tbx5+/+:MinKCre/+ (n=7)
Tbx3+/+:Tbx5+/+:MinKCreERT2/+
Tbx3F/+:Tbx5F/+:MinKCreERT2/+
Tbx3F/F:Tbx5F/F:MinKCreERT2/+
Tbx3F/F:Tbx5+/+:MinKCreERT2/+
Tbx3+/+:Tbx5F/F:MinKCreERT2/+
B
C
D
E
F
VCS-specific Tbx3:Tbx5 dCKO - histology
G
H
I
J
K
RA
LA
RV
LV
VCS-specific Tbx3:Tbx5 dCKO - qPCR analysis with fibrosis markers
L
gPCR Col1a1 expression level normalized to Gapdh
gPCR Postn expression level normalized to Gapdh
Col1a1
Postn
Tbx3+/+:Tbx5+/+:MinKCre/+ (n=3)
Tbx3F/+:Tbx5F/+:MinKCre/+ (n=3)
Tbx3F/F:Tbx5F/F:MinKCre/+ (n=3)
Tbx3F/F:Tbx5+/+:MinKCre/+ (n=3)
Tbx3+/+:Tbx5F/F:MinKCre/+ (n=3)

Figure 3.

Cardiac function is preserved following double-conditional loss of *Tbx3* and *Tbx5* in the adult ventricular conduction system (VCS).

(A) Left ventricular (LV) fractional shortening **(left graph)** and left ventricular (LV) ejection fraction **(right graph)** calculated from the M-mode ECGs in (B-F) revealed no contractile dysfunction in VCS-specific *Tbx3:Tbx5* double-conditional mutant mice (*Tbx3$^{fl/fl}$;Tbx5$^{fl/fl}$;R26$^{EYFP/+}$; MinK$^{CreERT2/+}$*). Data are presented as mean±SD. Welch *t* test: *P<0.05; ns, not significant; n=7 biological replicates/genotype. **(B-F)** Cardiac function, assessed by M-mode echocardiography from *Tbx3$^{+/+}$;Tbx5$^{+/+}$;R26$^{EYFP/+}$;MinK$^{CreERT2/+}$* **(B),** *Tbx3$^{fl/+}$;Tbx5$^{fl/+}$; R26$^{EYFP/+}$;MinK$^{CreERT2/+}$* **(C),** *Tbx3$^{fl/fl}$;Tbx5$^{fl/fl}$;R26$^{EYFP/+}$;MinK$^{CreERT2/+}$* **(D),** *Tbx3$^{fl/fl}$;Tbx5$^{+/+}$; R26$^{EYFP/+}$;MinK$^{CreERT2/+}$* **(E),** *Tbx3$^{+/+}$;Tbx5$^{fl/fl}$;R26$^{EYFP/+}$;MinK$^{CreERT2/+}$* **(F)** mice shown above surface ECGs. No functional differences between mutant and control mice were detected. The most representative images for each genotype were utilized in the figure. n=7 biological replicates/genotype. **(G-K)** Histological examination of all four-chambers from *Tbx3$^{+/+}$;Tbx5$^{+/+}$;R26$^{EYFP/+}$;MinK$^{CreERT2/+}$* **(G),** *Tbx3$^{fl/+}$;Tbx5$^{fl/+}$;R26$^{EYFP/+}$;MinK$^{CreERT2/+}$* **(H),** *Tbx3$^{fl/fl}$;Tbx5$^{fl/fl}$;R26$^{EYFP/+}$;MinK$^{CreERT2/+}$* **(I),** *Tbx3$^{fl/fl}$;Tbx5$^{+/+}$;R26$^{EYFP/+}$;MinK$^{CreERT2/+}$* **(J),** *Tbx3$^{+/+}$;Tbx5$^{fl/fl}$;R26$^{EYFP/+}$;MinK$^{CreERT2/+}$* **(K)** mice showed no histological abnormalities. The most representative images for each genotype were utilized in the figure. n=3-4 biological replicates/genotype. Boxed areas in (G-K) have been shown at higher magnification at their right sides. **(L)** qRT-PCR analysis for fibrosis genes *Col1a1* and *Postn* confirmed that there was no increase in expression of fibrosis markers in the VCS of *Tbx3:Tbx5*-deficient mice. Data are presented as mean±SD normalized to *Gapdh* and relative to *Tbx3$^{+/+}$;Tbx5$^{+/+}$;R26$^{EYFP/+}$;MinK$^{CreERT2/+}$* mice (set as 1). Welch *t* test: *P<0.05; ns, not significant; n=3 biological replicates/genotype (VCS cardiomyocytes pooled from 30 mice per each biological replicate). Histological examination original magnification: 2.5x, boxed area showed at the higher magnification: 40x.

To assess the hypothesis that *Tbx3* and *Tbx5* cooperatively promote VCS versus working myocardium phenotype, we conducted a transcriptional characterization of the adult VCS in *Tbx3$^{fl/fl}$;Tbx5$^{fl/fl}$;R26$^{EYFP/+}$;MinK$^{CreERT2/+}$* mutant mice compared to their *Tbx3$^{+/+}$;Tbx5$^{+/+}$;R26$^{EYFP/+}$;MinK$^{CreERT2/+}$* control littermates using three distinct sets of molecular markers by qRT-PCR (**Figure 4A-C**). The first set encompassed genes expressed throughout the entire conduction system (Pan-CCS) and implicated in slow-conducting nodal phenotype, such as *Hcn1, Hcn4, Cacna1d (Cav1.3), Cacna1g (Cav3.1d), Cacna1h (Cav3.2), Gjd3 (Cx30.2), and Gjc1 (Cx45)* (15, 30, 39–46) (**Figure 4A**). The second set included genes highly expressed in the fast-conducting VCS and important for VCS function, including *Gja5* (*Cx40), Scn5a (Nav1.5), Ryr2, Kcnk3 (Task-1), Kcnj2 (Kir2.1), Kcnj3 (Kir3.1), Kcnj4* (IRK3), and *Kcnj12 (Kir2.2)* (**Figure 4B**) (39, 40, 46–50). The third set contained markers specifically present in the working myocardium but absent in the CCS, such as *Gja1* (*Cx43)* and *Smpx* (**Figure 4C**) (30, 39, 51, 52). VCS-specific *Tbx3:Tbx5*-deficient mice lost VCS expression profile of genes required for the fast ventricular conduction (**Figure 4B**) as well as genes normally expressed in whole CCS (Pan-CCS genes) (**Figure 4A**). In contrast, these mice obtained VCS expression of working myocardium-specific molecular markers (**Figure 4C**). Immunoblotting analysis confirmed transcriptional changes observed by qRT-PCR (**Figure 4D**). This molecular characterization indicated that the *Tbx3:Tbx5* double mutant VCS adopted a gene expression profile similar to wild-type working myocardial-like cells (**Figure 4**).

The impact of the *Tbx3:Tbx5* double-conditional knockout on electrical impulse propagation in the VCS of the heart was assessed with optical mapping of the anterior epicardial surface of the ventricles and right septal preparations where VCS function should be observed (**Figure 5**). Optical mapping records changes in transmembrane potential from multiple cells in tissue preparations, where ventricular septal optical action potentials (OAP) have two distinct action potential upstrokes. The first peak is a result of depolarization of the specialized fast VCS, followed by depolarization of ventricular working myocardium.

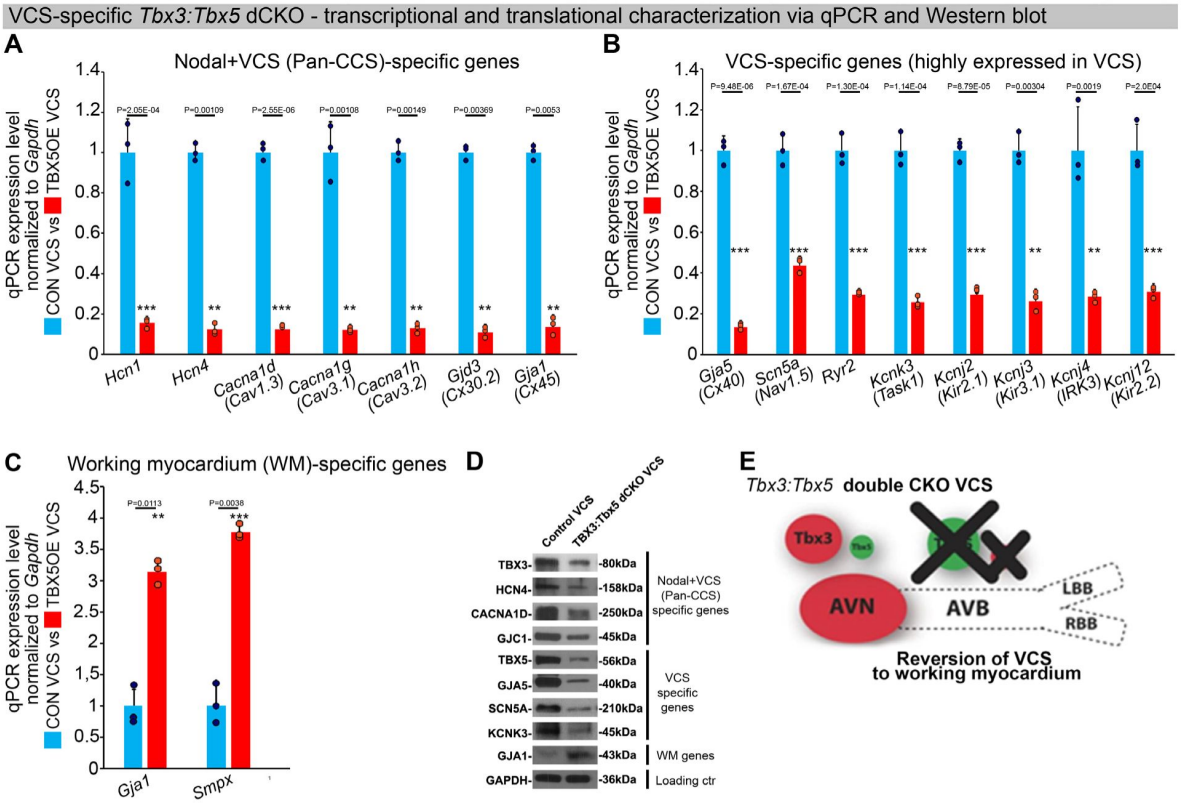

Figure 4.

In the adult murine heart, *Tbx3* and *Tbx5* cooperatively promote ventricular conduction system (VCS) versus working myocardium (WM) phenotype.

(A-C) qRT-PCR analysis of molecular changes driven by VCS-specific *Tbx3:Tbx5* double-conditional knockout in adult mice. Transcriptional characterization of the adult VCS in $Tbx3^{fl/fl};Tbx5^{fl/fl};R26^{EYFP/+};MinK^{CreERT2/+}$ mutant mice, compared to their $Tbx3^{+/+};Tbx5^{+/+};R26^{EYFP/+};MinK^{CreERT2/+}$ control littermates, was conducted using three distinct sets of molecular markers. **(A)** Genes expressed throughout the entire conduction system (Pan-CCS), implicated in the slow-conducting nodal phenotype. **(B)** Genes highly expressed in the fast-conducting VCS, critical for VCS function. **(C)** Markers specifically present in the working myocardium but absent in the CCS. VCS-specific *Tbx3:Tbx5*-deficient mice lost the VCS expression profile, including genes necessary for fast ventricular conduction **(B)** and those typically expressed in the entire CCS (Pan-CCS genes), essential for the slow conducting nodal phenotype **(A)**. In contrast, they acquired VCS expression of working myocardium-specific molecular markers important for working myocardial function **(C)**. **(D)** Immunoblotting analysis confirmed transcriptional changes indicated by qRT-PCR analysis **(A-C)** in VCS-specific *Tbx3:Tbx5* double-conditional knockout in adult mice. **(E)** Graphical summary of transcriptional changes observed in VCS of VCS-specific *Tbx3:Tbx5*-deficient mice. Simultaneous genetic deletion of *Tbx3* and *Tbx5* from the mature VCS resulted in a transcriptional profile resembling that of ventricular working myocardium. Data are presented as mean±SD normalized to *Gapdh* and relative to $Tbx3^{+/+};Tbx5^{+/+};R26^{EYFP/+};MinK^{CreERT2/+}$ mice (set as 1). Welch *t* test: *P<0.05; *P<0.005; *P<0.0005; n=3 biological replicates/genotype (VCS cardiomyocytes pooled from 30 mice per each biological replicate).

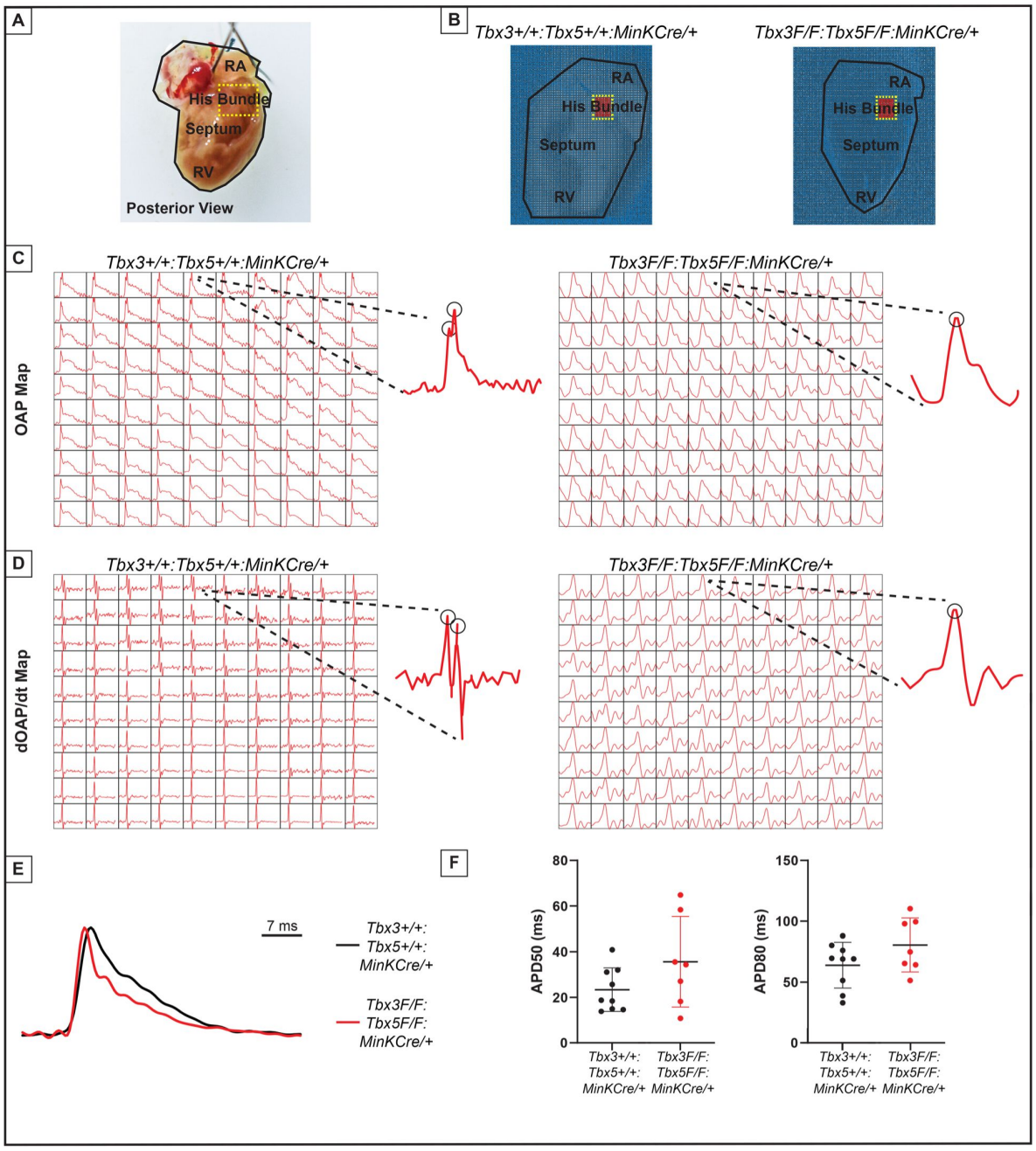

Figure 5.

Loss of VCS optical action potential (OAP) morphology in *Tbx3:Tbx5* double-conditional knockout mice.**(A)** Schematic of the posterior view of a mouse heart with right ventricle (RV) free wall removed, highlight the RV, septum, His bundle, and right atria (RA). **(B)** Representative 100×100 OAP map of OAP recorded during sinus rhythm from *Tbx3:Tbx*5 double-conditional knockout mice and control littermates with the free wall removed. Rge region of the His bundle is highlighted in red. **(C)** Representative 10×10 OAP map from the region of the His bundle. **(D)** Representative 10×10 map of the first derivative of the OAP from the region of the His bundle. **(E)** Representative ventricular OAP from whole heart intact preparation from *Tbx3:Tbx*5 double-conditional knockout mice (red) and control littermates (black). **(F)** Quantification of APD50 and APD80 at a basic cycle length of 125 ms.

To visualize electrical impulse propagation in *Tbx3:Tbx5* double-conditional knockout mice, a 100×100 pixel data frame was plotted for the entire field of view of the right septal preparation (**Figure 5A** and **B**). For enhanced analysis of the VCS, the region encompassing the His bundle was distinguished in a red 10×10 area (**Figure 5B**). To specifically assess electrical impulse propagation within the His bundle, the same 10×10 pixel area representing this region was isolated from adult hearts of both control and *Tbx3:Tbx5* double-conditional knockout mice (**Figure 5C**). We observed only one OAP upstroke in *Tbx3:Tbx5* double-conditional knockout mice in contrast to control mice which showed two OAP upstrokes. The first derivative of the OAP (dOAP/dt) from the region of the His bundle was calculated and plotted in a dOAP/dt map further highlighting the number of temporally distinct upstrokes within the OAP (**Figure 5D**). In control mice, we observed two distinct depolarization upstrokes, one pertaining to the VCS and the second for working ventricular myocardium. However, in *Tbx3:Tbx5* double-conditional knockout mice only one maximum dOAP/dt was observed (**Figure 5D**). The OAP morphology observed in *Tbx3:Tbx5* double-conditional knockout mice suggested a loss or reduction of the specialized fast VCS (**Figure 5C** and **D**).

OAPs from the anterior epicardial surface of the ventricles were compared between control littermates and *Tbx3:Tbx5* double-conditional knockout mice to assess changes in electrical impulse propagation in the ventricular working myocardium. Paced at a basic cycle length of 125 ms, control littermates and *Tbx3:Tbx5* double-conditional knockout mice did not exhibit significant differences in action potential duration at 50% (APD50) or 80% (APD80) repolarization (**Figure 5E** and **5F**). These observations suggested that the electrical activity of the ventricular working myocardium was not appreciably altered in double knockout mice compared to controls. This finding is consistent with the lack of changes in the ventricular effective refractory period (VERP) observed in invasive electrophysiology (EP) studies of both control and *Tbx3:Tbx5* double-conditional knockout mice (**Figure 3I**).

We further predicted that the double knockout would not affect action potentials or conduction properties distal to the VCS (**Figure 6**). OAP and dOAP/dt maps were created to observe the effects on electrical impulse propagation distal to the His bundle on the right septal preparation (**Figure 6**), similar to the methods applied to create OAP and dOAP/dt maps in the region of the His bundle (**Figure 5**), with the key difference being that the signals were recorded from the red 10×10 pixel regions plotted in the working ventricular myocardium distal to the His bundle instead of in the area of the His bundle (**Figure 6A** and **B** versus **Figure 5A** and **B**, respectively). In both control littermates and *Tbx3:Tbx5* double-conditional knockout mice, only one action potential upstroke and one dOAP/dt maximum are observed which indicates that most of this region consists of the ventricular working myocardium (**Figure 6C** and **D**, respectively). In summary, the significant remodeling of electrical impulse propagation due to *Tbx3:Tbx5* double-conditional knockout was observed by the loss of a distinct fast VCS impulse in the region of the His bundle, but not on the anterior epicardial surface of the ventricles or distal to the His bundle on the right ventricular septum (**Figure 5** and **6**).

Discussion

Our study investigated the impact of compound *Tbx3:Tbx5*-deficiency on mature VCS function and molecular identity. Using a double-conditional knockout strategy, both genes were targeted specifically in the adult VCS. Loss of *Tbx3* and *Tbx5* expression in the mature VCS led to profound conduction defects, characterized by prolonged PR interval and QRS duration, increased susceptibility to ventricular tachycardia, and sudden death. These alterations were observed in the absence of discernible changes in cardiac contractility or histological morphology, indicating a primary conduction system defect. Molecular characterization of the adult VCS unveiled an altered gene expression profile in *Tbx3:Tbx5* double-conditional knockout mice, suggesting a transition from the distinctive fast VCS transcriptional profile to that resembling ventricular working

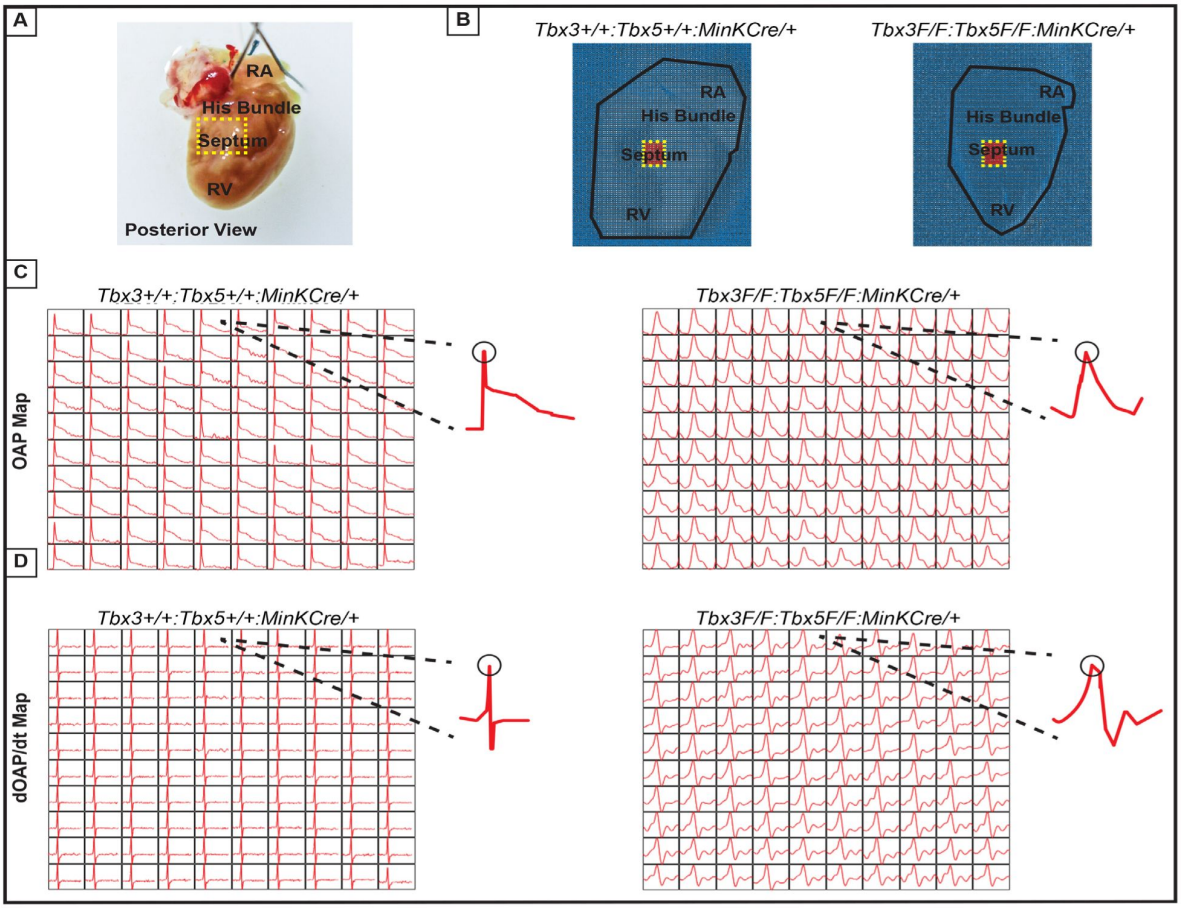

Figure 6.

Ventricular optical action potentials (OAPs) distal from His bundle have only 1 OAP upstroke.
(A) Schematic of the posterior view of mouse heart with right ventricle (RV) free wall removed. **(B)** Representative 100×100 pixel OAP map recorded during sinus rhythm from *Tbx3:Tbx*5 double-conditional knockout mice and control littermates with RV free wall removed. The region of the working ventricular myocardium distal from the His bundle is highlighted in red. **(C)** Representative 10×10 pixel OAP map from the region distal to the His bundle. **(D)** Representative 10×10 dOAP/dt map from the region distal to the His bundle.

myocardium. Optical mapping demonstrated loss of the specialized fast VCS function in *Tbx3:Tbx5* double-conditional knockout mice, further suggesting that this region acquired an electrophysiological phenotype similar to the ventricular working myocardium.

Our previous research (1, 3, 11, 12) and published literature (7, 15, 20, 26, 53, 54) have suggested that the balance between *Tbx3* and T*bx5* expression determines the regional patterning of the mature central cardiac conduction system (**Figure 7**). *Tbx3* expression dominates in nodal myocardium, imparting nodal physiologic characteristics. *Tbx5* expression dominates in fast VCS myocardium, where a T-box-dependent fast conduction system network drives physiologically dominant fast conduction physiology, overriding nodal physiology (11) (**Figure 7**). This model accurately predicts the outcome of targeted manipulations such as adult VCS-specific removal of TBX5 or overexpression of TBX3, in which fast VCS is re-patterning into a slow nodal-like system (11) (**Figure 7**).

The CCS patterning model predicts that *Tbx3* and *Tbx5* coordinately pattern the CCS and suggests their compound necessity for specialized VCS fate (**Figure 7**), a hypothesis that remained untested. This model predicted that VCS-specific genetic ablation of both the TBX3 and TBX5 transcription factors would transform fast-conducting adult VCS into cells resembling working myocardium, eliminating specialized CCS fate (**Figure 7**). Testing this model necessitated the generation of a *Tbx3:Tbx5* double-conditional knockout allele due to their proximal chromosomal location in *cis* on mouse Chr5. VCS-specific double knockout mice showed a notable deceleration in VCS conduction, manifested by prolonged PR and QRS intervals, along with increased susceptibility to ventricular tachycardia (VT). A similar functional phenotype was observed in single deletion of *Tbx5* from the adult VCS, leading to the transformation of the fast VCS into a nodal-like phenotype (1, 11). However, we predicted that the nodal-like characteristics of the *Tbx5*-ablated VCS were due to retained expression of *Tbx3*. In fact, the autonomous beating and impulse initiation observed in the *Tbx5*-mutant VCS (1, 11) were absent from the double *Tbx3:Tbx5* mutant VCS, further suggesting the transformation from a nodal-like to an inert myocardial functionally and a fate transformation from conduction to simple working myocardium.

Molecular studies support a transformation from conduction to working myocardium in the *Tbx5:Tbx3* double VCS knockout. Previous studies investigating the roles of *Tbx3* and *Tbx5* in adult VCS specification demonstrated that *Tbx3* deletion resulted in the silencing of Pan-CCS gene expression in the atrioventricular conduction system (7, 15, 20, 26, 53). Alternately, specific deletion of *Tbx5* from the adult VCS led to the repression of VCS-specific markers while Pan-CCS markers remained unchanged, indicating a transformation towards a nodal-like transcriptional phenotype in the absence of *Tbx5* (1, 11). Consistently, a similar transformation was induced by *Tbx3* overexpression in the adult VCS. These findings underscored the significance of the *Tbx3:Tbx5* ratio in the molecular and functional patterning of the fast versus slow conduction system. In *Tbx3:Tbx5* double VCS knockout, we observed repression of fast VCS markers and also repression of Pan-CCS markers transcribed throughout the entire CCS. As expected, not all VCS markers were ablated in VCS-specific *Tbx3:Tbx5* mutants. A significant portion of VCS fast conduction markers are also transcribed in ventricular working myocardium, albeit at lower levels than in the VCS, and are crucial for normal working myocardial function, e.g., *Ryr2, Scn5a,* and *Kcnj2* (39, 46, 49). Consistent with a shift from fast VCS to working myocardium, their expression levels are present, but at significantly lower levels in the double knockout mutants than in normal VCS. Furthermore, the expression of markers specific for working myocardium, which are normally excluded in the VCS, emerged in the VCS of *Tbx3:Tbx5* double mutant. These observations are consistent with a transcriptional shift from VCS conduction cardiomyocytes to working myocardium-like characteristics in the absence of both *Tbx3* and *Tbx5*.

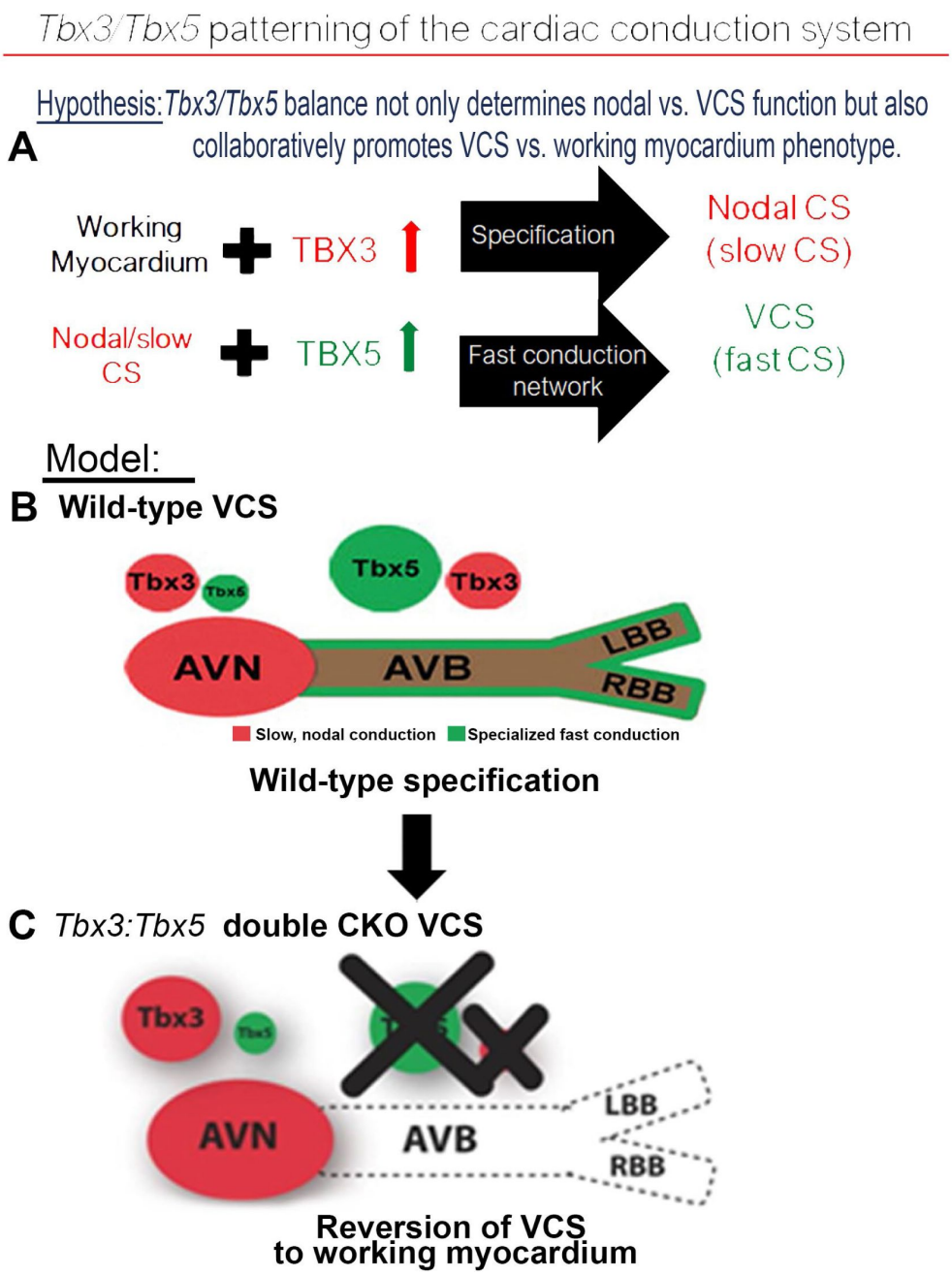

Figure 7.

Tbx3 and *Tbx5* play distinct roles in the adult VCS while cooperatively promoting CCS regional specification—a model elucidating our hypothesis for *Tbx5/Tbx3* dose-dependent CCS regional specification.
(A) The *Tbx3/Tbx5* balance not only governs nodal versus ventricular conduction system (VCS) function but also collaboratively promotes the VCS versus working myocardium (WM) phenotype. Specifically, a high level of *Tbx3* is linked to the specification to the nodal conduction system, while an elevated *Tbx5* level in nodal cells activates local expression of the *Tbx5*-dependent fast conduction network, resulting in the generation of VCS. **(B)** CCS regional specialization is driven by local expression of *Tbx5*-dependent fast conduction network in the VCS, which overlaps underlying Pan-CCS expression of nodal, slow conduction network. **(C)** VCS-specific simultaneous genetic removal of both the *Tbx3* and Tbx5 transcription factors transforms the fast-conducting, adult VCS into cells resembling working myocardium, thereby re-patterning them from conduction to non-conduction myocytes. Therefore, within the adult CCS, the *Tbx3* and *Tbx5* expression levels are crucial not only for normal fast versus slow patterning but also for maintaining the conduction versus contraction specification of the VCS.AVB indicates atrioventricular bundle; AVN, atrioventricular node; CCS, cardiac conduction system; CKO, conditional KO; LBB, left bundle brunch; RBB, right bundle brunch; VCS, ventricular conduction system.

Optical mapping provided further evidence in favor of the transformation from VCS to working myocardium in the absence of both *Tbx3* and *Tbx5*. We observed the loss of fast VCS in the region of the His bundle in the *Tbx3:Tbx5* double-conditional knockout mice, indicated by presence of only one upstroke in the OAP in the region of the His bundle and VCS. The homogenous morphological and molecular transformation of His bundle and VCS cells in the *Tbx3:Tbx5* double-conditional knockout mice resulted in the electrical properties of the VCS-located cells being functionally indistinguishable from that of the ventricular cells. Thus, the electrical impulse propagation in the ventricles is slowed, now activating in a manner similar to exogenous pacing rather than rapid impulse propagation through the VCS.

Here, we have shown that *Tbx3* and *Tbx5* are cooperatively responsible for the patterning of the fast conduction VCS versus the non-specialized ventricular working myocardium (**Figure 7**). Deletion of both transcription factors from the VCS resulted in characteristics resembling ventricular working myocardium. This study combined with prior literature (1, 7, 11, 15, 26, 53, 54) indicates that the presence of both *Tbx3* and *Tbx5* is necessary for the specification of the adult VCS (**Figure 7**).

Methods

Data Availability

The authors declare that all supporting data and materials presented within this manuscript and its Online Supplemental Materials are available from the corresponding author upon reasonable request.

Experimental animals

All animal experiments were performed under the University of Chicago Institutional Animal Care and Use Committee (IACUC) approved protocol (ACUP no. 71737) and in compliance with the USA Public Health Service Policy on Humane Care and Use of Laboratory Animals. $MinK^{CreERT2}$ [*Tg(RP23-276I20-MinkCreERT2)*] and $Tbx3^{fl/fl}$ mice have been reported previously (8, 26).

Tbx3:Tbx5 double floxed mouse line was generated by University of Utah Core Research Facility using CRISPR/Cas9. Guide RNA (sgRNA) constructs were designed with software tools (ZiFiT Targeter (55) and *crispr.genome-engineering.org*) predicting unique target sites throughout the mouse genome (Supplementary Figure 3 - 5). The sgRNA constructs were transcribed *in vitro* using MEGAshortscript T7 (Invitrogen AM1354) and mMessage Machine T7 transcription kit (Invitrogen AM1344) according to manufacturer instructions. The strategy to generate mouse founders involved a single-step microinjection into one-cell *Tbx3* floxed zygotes (on a mixed background) with 10 ng/μL of each sgRNA (TBX5-I2-S22 and TBX5-I3-S31, Supplementary Figure 3 - 5), 30 ng/μL of Cas9 protein, and 10 ng/μL of a long ssDNA donor. The donor contained two lox2272 sites in cis, spanning partial intron 2, entire exon 3, and partial intron 3 of the mouse *Tbx5* gene, along with 100/150 bp 5'/3' homology arms (Supplementary Figure 4).Founders were validated by PCR, restriction enzyme digestion, and Sanger sequencing (Supplementary Figure 1B, C, and D). Founders were backcrossed with wild-type *CD1 IGS* mice (Charles River Lab, USA) to confirm germline transmission of the *CRISPR/Cas9*-generated compound *Tbx3:Tbx5* double-floxed allele and obtain the F1 generation. F1 mice were then interbred to establish a stable *Tbx3:Tbx5* double-floxed mouse line. Downstream experiments were performed on F4-F6 mice.

To simultaneously conditionally delate the *Tbx3* and *Tbx5* genes specifically from the adult VCS, we crossed our *Tbx3:Tbx5* double-floxed mouse line ($Tbx3^{fl/fl}$;$Tbx5^{fl/fl}$) with a VCS-specific tamoxifen (TM) inducible *Cre* transgenic mouse line ($MinK^{CreERT2}$ [Tg(RP23-276I20-MinkCreERT2; (8)) (**Figure 1A**). All mice were maintained on a mixed genetic background. Tamoxifen (MP Biomedical) was administered at a dose of 0.167 mg/g body weight for 5 consecutive days by oral

gavage at 6 weeks of age and then mice were evaluated at 9 weeks of age, as previously described (1, 8, 11). Age-, gender-, and genetic strain-matched controls were used in all experiments to account for any variations in data sets across experiments. Mice were bred and housed in specific pathogen–free conditions in a 12-hour light/12-hour dark cycle and allowed ad libitum access to standard mouse chow and water. Mice requiring medical attention were provided with appropriate veterinary care by a licensed veterinarian and were excluded from the experiments described. No other exclusion criteria were applied.

All experiments and subsequent analysis were conducted in a blinded fashion, with animals randomly assigned to experimental groups. Following genotyping, mice were randomly allocated to the studies based on their genotypes. Subsequently, their identities were anonymized using a numerical code to ensure that all experiments and analyses were performed in a blinded manner. Both, male and female animals have been used in our studies in the ratio of 41%/59%, based on availability of relatively rare compound genotypes, respectively.

Echocardiography studies

Transthoracic echocardiography in mice was conducted under inhaled isoflurane anesthesia administered through a nose cone. Prior to imaging, chest hairs were removed using a topical depilatory agent. Limb leads were affixed for electrocardiogram gating, and animals were imaged in the left lateral decubitus position with a VisualSonics Vevo 770 machine using a 30-MHz high-frequency transducer. To ensure stability, body temperature was carefully maintained using a heated imaging platform and warming lamps. Two-dimensional images were meticulously recorded in parasternal long- and short-axis projections, accompanied by guided M-mode recordings at the midventricular level in both views. Left ventricular (LV) cavity size and percent fractional shortening were measured in at least 3 beats from each projection and averaged. M-mode measurements were employed to ascertain LV chamber dimensions and percent LV fractional shortening, calculated as ([LVIDd – LVIDs]/LVIDd), where LVIDd and LVIDs represent LV internal diameter in diastole and systole, respectively.

Surface electrocardiography (ECG)

9 weeks old, tamoxifen treated control and mutant mice were anesthetized with a mixture of 2-3% isoflurane in 100% oxygen. Anesthetized mice were secured in a supine position on a regulated heat pad while lead I and lead II ECGs were recorded using platinum subdermal needle electrodes in a 3-limb configuration. Core temperature was continuously monitored using a rectal probe and maintained at 36–37 °C throughout the procedure. ECG data were collected and analyzed using Ponemah Physiology Platform (DSI) software and an ACQ-7700 acquisition interface unit (Gould Instruments, Valley View, OH, USA). Key parameters derived from the ECG measurements included: Heart rate (HR), PR interval (from the beginning of the P wave to the beginning of the QRS complex), and QRS complex duration.

Telemetry ECG analysis

9 weeks old, tamoxifen treated control and mutant mice were anesthetized with 2-3% isoflurane in 100% oxygen, and wireless telemetry transmitters (ETA-F10; DSI) were surgically implanted in the back with leads tunneled to the right upper and left lower thorax, as previously described (1, 56). Following 24-hour recovery period after surgical instrumentation, heart rate and PR and QRS intervals were calculated using Ponemah Physiology Platform (DSI) from 48-hour recordings.

Catheter-based intracardiac electrophysiology

Detailed protocols for invasive electrophysiology studies (EP) have been previously described (57, 58). Briefly, 9 weeks old, tamoxifen treated control and mutant mice were anesthetized using 2-3%isoflurane in 100% oxygen. Then, a 1.1-Fr octapolar electrode catheter (EPR-800; Millar Instruments) was advanced via a right jugular venous cut-down to record right atrial (RA), His

bundle, and right ventricular (RV) potentials, as well as to perform programmed electrical stimulation. Signals were identified through alignment with simultaneous surface electrocardiography (ECG) using subcutaneous needle electrodes in a Lead II configuration. “Near-Field” and “Far-Field” signals were identified based on ECG alignment, signal deflection upstroke speed and total signal duration. Standard tachycardia induction protocols included an 8-beat drive train with beats 80-120ms apart (S1), followed by 5 beats (S2) at 50ms apart (penta-extrastimulus, PES). Two attempts at this PES protocol were carried out. Mice also underwent single extrastimulus testing (SES) with 8 beats 80-120ms apart (S1) followed by a single S2 at 50ms. This SES protocol was carried out 5 separate times per mouse. If these two protocols in the right atrium and right ventricle (separately) failed to initiate their respective tachycardias, the study was deemed negative. S1 drive train intervals varied slightly due to the presence of the AV Wenckebach block at faster pacing rates in some mice; the S1 interval was lengthened to prevent this during the drive train.

Additional atrial and ventricular pacing protocols were carried out to obtain atrial, atrio-ventricular, and ventricular effective refractory periods (AERP, AVERP, VERP) as well as sinus node recovery time, as described previously (57–60). Effective refractory periods were measured using 8-beat S1 drive trains of 100 ms followed by single extra-stimulus.

ECG and Optical mapping

Electrocardiogram (ECG) Acquisition and Analysis

ECGs were recorded in conscious *Tbx3:Tbx5* double-conditional knockout mice and control littermates using the ecgTUNNEL device (emka Technologies) 2 weeks after tamoxifen treatment. Mice were positioned in the tunnel and ECGs were recorded for 5 minutes at a sampling rate of 1 kHz using lead I. ECGs were analyzed using a custom MATLAB program to measure P, and QRS durations, as well as PR, QT and RR intervals (61, 62) (Supplementary Figure 6).

Langendorff Perfusion

Tbx3:Tbx5 double-conditional knockout mice (n=8) and control littermates (n=10) were deeply anesthetized with isoflurane. The heart was quickly excised following cervical dislocation and thoracotomy. The aorta was cannulated, and the heart was retrogradely perfused with warmed (37°C) and oxygenated (95% O2 and 5% CO2) modified Tyrode’s solution (in mM, NaCl 130, NaHCO3 24, NaH2PO4 1.2, MgCl2 1, Glucose 5.6, KCl 4, and CaCl2 1.8) at a pH of 7.4. The heart was placed in a constant-flow (1.0 - 2.0 ml/min) Langendorff Perfusion system, laying horizontally in a tissue bath.

Ventricular Optical Mapping

The Langendorff Perfused heart was electromechanically uncoupled by 15 μM of blebbistatin (Cayman Chemicals 13186) perfusion. A voltage-sensitive fluorescent dye, 80 μM di-4-ANEPPs (ThermoFisher Scientific D1199), was administered through the dye injection port. The heart was illuminated using a 520 ± 5 nm (Prizmatix, UHP-Mic-LED-520) wavelength light source to excite di-4-ANEPPs. Emitted photons were captured using complementary metal-oxide semiconductor (CMOS) cameras (MiCAM, SciMedia). The stimulation threshold, where the heart would capture the stimuli and action potential 1:1, was determined using a point source platinum electrode placed on the anterior surface of the heart on the anterior epicardial surface of the ventricles. Pacing was applied at 1.5x the threshold amplitude to maintain 1:1 capture over the duration of the experiment. Optical recordings were analyzed using Rhythm 1.2 to analyze transmembrane potential (63). Action potential duration (APD) at 50% and 80% repolarization were calculated for the ventricles of the intact whole heart preparation.

Right Septal Preparation Optical Mapping Experiments

Following intact whole heart *ex vivo* optical mapping, the heart was removed from the tissue bath for the dissection of the right ventricular (RV) free wall to expose the RV septal surface (64). The heart was quickly returned to the tissue bath and the RV septal surface was focused into the field of view. Sinus rhythm optical recordings were acquired.

A custom MATLAB program was written to plot individual pixels in a 100×100-pixel image stack. A Butterworth filter of order 5 was applied to provide temporal filtering (65). The location of the His bundle was identified as the region at the base of the interventricular septum (a red 10×10 pixel area in **Figure 5B**). Signals from the working ventricular myocardium were recorded from the 10×10 pixel region plotted in the working ventricular myocardium distal to the His bundle (**Figure 6B**).

Isolation of adult VCS cardiomyocytes and cell sorting

To isolate EYFP-positive VCS cardiomyocytes, a tip of ventricular septum below the AV annulus was microdissected out from 9 weeks old TM-treated control and *Tbx3:Tbx5* double-conditional mutant mice (1, 2, 66) under a fluorescence dissecting scope. Single-cell fluorescent-activated cell sorting (FACS) samples were prepared as previously described (67). Propidium iodide (ThermoFisher Scientific) was added immediately before FACS to facilitate live/dead discrimination. Cells were sorted on a FacsAria flow cytometer (BD Biosciences) located at the University of Chicago Flow Cytometery Core using Influx software. Samples from wild-type age-matched hearts were used for gating. Samples were gated to exclude debris and cell clumps. Fluorescent cells were collected into ice-cold RNase-free PBS and processed for RNA extraction.

RNA isolation and QRT-PCR

Total RNA was extracted from EYFP-positive VCS cardiomyocytes obtained by sorting from 9 weeks old control and VCS-specific *Tbx3:Tbx5*-deficient mice using RNeasy Mini Kit (Qiagen), followed by DNase treatment according to the manufacturer's instructions. Reverse transcription reaction was carried out using the SuperScript III First-Strand Synthesis SuperMix for quantitative RT-PCR (Invitrogen) as per the manufacturer's recommendations. QRT-PCR was performed using the POWER SYBR Green PCR master mix from Applied Biosystems and run on an Applied Biosystems AB7500 machine in 96 well plates. The relative gene expression level was calculated by the ΔΔCt method (68) using glyceraldehyde-3-phosphate dehydrogenase (Gapdh) gene expression level as internal control. The data presented are the average of three independent experiments.

Protein isolation and Western blotting

Atria and ventricles were dissected from *Tbx3:Tbx5* mutant mice (*Tbx3*$^{fl/fl}$;*Tbx5*$^{fl/fl}$;*R26*$^{EYFP/+}$;*MinK*$^{CreERT2/+}$)and their littermate controls *Tbx3*$^{+/+}$;*Tbx5*$^{+/+}$;*R26*$^{EYFP/+}$; *MinK*$^{CreERT2/+}$) littermates that had been administered tamoxifen at 6-7 weeks of age and studied 4-5 weeks following tamoxifen administration. The tissues were snap-frozen in liquid nitrogen, pulverized, and homogenized in RIPA buffer (50 mM Tris-HCl pH 8, 150 mM NaCl, 1% Triton-X, 0.5% sodium deoxycholate, 0.1% SDS, 5 mM EDTA) with 1 Roche EDTA-Free complete protease inhibitor tablet per 50 mL of buffer. Samples were tumbled for 1 hour at 4°C and then centrifuged for 10 minutes at 13,200 x g. Protein concentration was determined using the BCA assay (Pierce) with BSA as a standard. For Western blot analysis, 25 µg of protein was diluted in Laemmli buffer, heated at 70°C for 10 minutes, and subjected to SDS-PAGE on 4-20% TGX gels (Bio-Rad). Proteins were then transferred to nitrocellulose membranes, blocked with 5% milk in TBS-T, and incubated overnight at 4°C with primary antibodies diluted in 2.5% milk in TBS-T. The primary antibodies used were: goat polyclonal anti-TBX3 (Santa Cruz Biotechnology, sc-31656, 1:250), rabbit polyclonal anti-HCN4 (Millipore, AB5808, 1:500), rabbit polyclonal anti-CAV1.3/CACNA1D (Alomone, ACC-005, 1:200),

rabbit polyclonal anti-Cx45/GJC1 (Thermo Fisher, PA5-77357, 1:250), sheep polyclonal anti-TBX5 (R&D, AF5918, 1:200), rabbit polyclonal anti-CX40/GJA5 (Zymed/Invitrogen, 36-4900, 1:500), rabbit polyclonal anti-NAV1.5/SCN5A (Alomone, ASC-005, 1:200), mouse monoclonal anti-KCNK3/TASK1 (Abcam, ab186352, 1:1000), rabbit polyclonal anti-CX43/GJA1 (Cell Signaling Technology, 3512, 1:1000), and mouse monoclonal anti-GAPDH (Abcam, ab8245, 1:1000). After rinsing in TBS-T, membranes were incubated for one hour at RT with secondary antibodies diluted in 2.5% milk in TBS-T, rinsed again, and visualized using enhanced chemiluminescence reagents (Pierce ECL/ECL Plus, Thermo Fisher Scientific) and Kodak X-OMAT film. Results were normalized to GAPDH loading control and then quantified using ImageJ software (69, 70). Secondary antibodies used were donkey anti-goat IgG AlexaFluor-594 (Invitrogen, A-11058, 1:250 dilution) and donkey anti-goat IgG AlexaFluor-488 (Invitrogen, A-11055, 1:250 dilution) for experiments involving co-staining for goat primary antibodies. Secondary antibodies were as follows: rabbit anti-goat-HRP (Jackson ImmunoResearch, 305-035-003, 1:10 000), goat anti-rabbit-HRP (Jackson Immuno120 Research, 111-035-144, 1:3000), donkey anti-sheep-HRP (Ab cam, ab6900, 1:5000), and sheep anti-mouse-HRP (Amersham GE, NA931, 1:2500).

Histology

Hearts from 9-week-old control and mutant mice were carefully dissected, flushed with ice-cold PBS, and then fixed for 48 hours at 4 °C in a 4% paraformaldehyde solution (Sigma-Aldrich). Following fixation, the hearts were processed for paraffin-embedded sections and subjected to analysis through H&E staining, following the manufacturer's protocol provided by Sigma-Aldrich.

Immunofluorescence

Hearts from 9 weeks old control and mutant mice were dissected out and placed in ice-cold PBS, followed by freezing in OCT (Fisher) within the gas phase of liquid nitrogen. Cryosections of 7 µm thickness were mounted onto Superfrost Plus glass slides (Fisher Scientific), air-dried, and fixed for 10 minutes in ice-cold 4% paraformaldehyde (Sigma-Aldrich). Subsequently, sections were permeabilized in 1% Triton-X100 (Sigma-Aldrich) in PBS for 10 min, then blocked in 10% normal goat serum (Invitrogen) in PBS-T (PBS+0.1% Tween-20) for 30 min at room temperature (RT). Sections were then incubated overnight at 4°C in primary antibody diluted in blocking buffer, rinsed in PBS, then subsequently incubated for 60 min at RT in secondary antibody diluted in blocking buffer. Slides were mounted in VectaShield+DAPI (Vector Laboratories) or counterstained with DAPI and mounted in ProLog Gold (Invitrogen) priori to visualizing fluorescence. Primary antibodies were as follows: goat polyclonal anti-TBX3 (Santa Cruz, sc-31656, 1:250 dilution) and goat polyclonal anti-TBX5 (Santa Cruz, sc-17866, 1:250 dilution). Secondary antibodies used were donkey anti-goat IgG AlexaFluor-594 (Invitrogen, A-11058, 1:250 dilution) and donkey anti-goat IgG AlexaFluor-488 (Invitrogen, A-11055, 1:250 dilution) for experiments involving co-staining for goat primary antibodies. A secondary antibody-only control was employed in each case to ensure the specificity of immunostaining.

Statistics

The numbers of independent experiments are specified in the relevant figure legends. Quantitative data are presented as mean ± SD. Statistical analysis was performed using R version 3.6.2. or the GraphPad Prism statistical package version 10.2.1 (GraphPad Software, Boston, MA, USA). All data sets were analyzed independently for normality using Shapiro-Wilk normality test. If samples presented a normal distribution, the two-sample Welch t-test was performed. If normal distribution was not present, the non-parametric Mann-Whitney U test or Kruskal-Wallis H test was used, as indicated in the text. Statistical significance was assumed if P reached a value ≤ 0.05. The multiple comparison correction tests were performed on VCS, atrial and ventricular qRT-PCR data by calculation the false discovery rate (FDR) using the Benjamini & Hochberg procedure (71). A significant group-mean was considered at FDR<0.05.

Additional information

Sources of Funding

This work was supported by National Institutes of Health (R01 HL126509, R01 HL148719, R01 HL147571, and R33 HL123857 to I.P. Moskowitz), Foundation Leducq Transatlantic Networks of Excellence (to I.P. Moskowitz), and American Heart Association (7CSA33610126 to I.P. Moskowitz and 13POST17290028 to O. Burnicka-Turek).

Conflict of Interest Statement

None declared.

Contributions

IPM and OBT conceived and designed the study; OBT, KAT, BL, MTB, ZK, ER, BL, ES, MG, KMS, and DEA performed wet lab experiments; OBT, KAT, BL, MTB, MG, KMS, IRE, and IPM participated in data analysis. IPM directed the project; OBT and IPM drafted the manuscript. OBT and IPM serve as co-corresponding authors. All authors contributed to the final manuscript.

Nonstandard Abbreviations and Acronyms

- ACUP: animal care and use protocol
- AERP: atrial effective refractory period
- A-H: atrio-hisian interval
- APD50, 80: action potential duration at 50 and 80% of repolarization
- AVB: atrioventricular bundle
- AVERP: atrioventricular nodal effective refractory period
- AVN: atrioventricular node
- BBs: bundle branches
- *Cacna1d/Cav1.3*: calcium channel, voltage-dependent, L type, alpha 1D subunit
- *Cacna1g/Cav3.1d*: calcium channel, voltage-dependent, T type, alpha 1G subunit
- *Cacna1h/Cav3.2*: calcium channel, voltage-dependent, T type, alpha 1H subunit
- CCS: cardiac conduction system
- Chr5: chromosome 5
- *Col1a1*: collagen, type I, alpha 1
- CREs: *cis*-regulatory elements
- CRISPR: clustered regularly interspaced short palindromic repeats
- EP studies: electrophysiology studies
- ECG: electrocardiography
- *Eyfp*: enhanced yellow fluorescent protein
- FACS: fluorescent-activated cell sorting
- FDR: False Discovery Rate
- FS: fractional shortening
- *Gja1/Cx43*: gap junction protein, alpha 1
- *Gja5/Cx40*: gap junction protein, alpha 5
- *Gjc1/Cx45*: gap junction protein, gamma 1
- *Gjd3/Cx30.2*: gap junction protein, delta 3
- GRN: gene regulatory network
- GWAS: genome wide association studies
- *Hcn1*: hyperpolarization activated cyclic nucleotide gated potassium channel 1

- *Hcn4*: hyperpolarization-activated, cyclic nucleotide-gated K+ 4
- Hd: his-duration
- HOS: Holt-Oram syndrome
- H-V: hisio-ventricular interval
- IACUC: institutional animal care and use committee
- *Kcne1/MinK*: potassium voltage-gated channel, Isk-related subfamily, member 1
- *Kcnj2/Kir2.1*: potassium inwardly-rectifying channel, subfamily J, member 2
- *Kcnj3/Kir3.1*: potassium inwardly-rectifying channel, subfamily J, member 3
- *Kcnj4*/IRK3: potassium inwardly-rectifying channel, subfamily J, member 4
- *Kcnj12/Kir2.2*: potassium inwardly-rectifying channel, subfamily J, member 12
- *Kcnk3/Task-1*: potassium channel, subfamily K, member 3
- lssDNA donor: long single-stranded DNA donor
- LVEF: left ventricular ejection fraction
- OAP: optical action potential
- OE: overexpression
- OMIM: online Mendelian inheritance in man
- QRS: QRS complex
- QT: QT-interval duration
- PAM sequence: protospacer-adjacent motif sequence
- *Postn*: periostin, osteoblast specific factor
- PR: PR-interval duration
- RFLP: Restriction fragment length polymorphism
- *RR*: RR-interval duration
- *Ryr2*: ryanodine receptor 2, cardiac
- SAN: sinoatrial node
- *Scn5a*/*Nav1.5*: sodium channel, voltage-gated, type V, alpha
- sgRNA: single guide RNA
- Smpx: small muscle protein, X-linked
- *Tbx3*: T-box 3
- *Tbx5*: T-box 5
- TM: tamoxifen
- VCS: ventricular conduction system
- VERP: ventricular effective refractory period
- VT: ventricular tachycardia

References

1. Arnolds D.E., Liu F., Fahrenbach J.P., Kim G.H., Schillinger K.J., Smemo S., McNally E.M., Nobrega M.A., Patel V.V., Moskowitz I.P. (2012) **TBX5 drives Scn5a expression to regulate cardiac conduction system function** *J Clin Invest* **122**:2509–2518

2. Park D.S., Fishmann G.I. (2011) **The cardiac conduction system** *Circulation* **123**:904–915

3. Moskowitz I.P.G. *et al.* (2007) **A molecular pathway including Id2, Tbx5, and Nkx2-5 required for cardiac conduction system** *Development. Cell* **129**:1365–1376

4. Munshi N.V. (2012) **Gene Regulatory Networks in Cardiac Conduction System Development** *Circ Res* **110**:1525–1537

5. Rubart M., Zipes D.P. (2005) **Mechanisms of sudden cardiac death** *J Clin Invest* **115**:2305–2315

6. Huikuri H.V., Castellanos A., Myerburg R.J. (2001) **Sudden death due to cardiac arrhythmias** *N Engl J Med* **345**:1473–1482

7. van Duijvenboden K., Ruijter J.M., Christoffels V.M. (2014) **Gene regulatory elements of the cardiac conduction system** *Brief Funct Genomics* **13**:28–38

8. Arnolds D.E., Moskowitz I.P. (2011) **Inducible recombination in the cardiac conduction system of minK:CreERT2 BAC transgenic mice** *Genesis* **49**:878–884

9. Scheinman M.M. (2009) **Role of the His-Purkinje system in the genesis of cardiac arrhythmia** *Heart Rhythm* **6**:1050–10158

10. Arnolds D.E., Chu A., McNally E.M., Nobrega M.A., Moskowitz I.P. (2011) **The emerging genetic landscape underlying cardiac conduction system function** *Birth Defects Res A Clin Mol Teratol* **91**:578–585

11. Burnicka-Turek O. *et al.* (2020) **Transcriptional Patterning of the Ventricular Cardiac Conduction System** *Circ Res* **127**:e94–e106

12. Moskowitz I.P., Pizard A., Patel V.V., Bruneau B.G., Kim J.B., Kupershmidt S., Roden D., Berul C.I., Seidman C.E., Seidman J.G. (2004) **The T-Box transcription factor Tbx5 is required for the patterning and maturation of the murine cardiac conduction system** *Development* **131**:4107–4116

13. van Weerd J.H., Christoffels V.M. (2016) **The formation and function of the cardiac conduction system** *Development* **143**:197–210

14. van den Boogaard M. *et al.* (2012) **Genetic variation in T-box binding element functionally affects SCN5A/SCN10A enhancer** *J Clin Invest* **122**:2519–2530

15. Bakker M.L. *et al.* (2012) **T-box transcription factor TBX3 reprogrammes mature cardiac myocytes into pacemaker-like cells** *Cardiovasc Res* **94**:439–449

16. Hatcher C.J., Basson C.T. (2009) **Specification of the cardiac conduction system by transcription factors** *Circ Res* **105**:620–630

17. Bakker M.L., Boukens B.J., Mommersteeg M.T., Brons J.F., Wakker V., Moorman A.F., Christoffels V.M. (2008) **Transcription factor Tbx3 is required for the specification of the atrioventricular conduction system** *Circ Res* **102**:1340–1349

18. Hoogaars W.M. *et al.* (2007) **Tbx3 controls the sinoatrial node gene program and imposes pacemaker function on the atria** *Genes Dev* **21**:1098–1112

19. Mori D.A. *et al.* (2006) **Tbx5-dependent rheostatic control of cardiac gene expression and morphogenesis** *Dev Biol* **297**:566–586

20. Bruneau B.G. *et al.* (2001) **A murine model of Holt-Oram syndrome defines roles of the T-box transcription factor Tbx5 in cardiogenesis and disease** *Cell* **106**:709–721

21. Hoogaars W.M., Barnett P., Moorman A.F., Christoffels V.M. (2007) **T-box factors determine cardiac design** *Cell Mol Life Sci* **64**:646–660

22. Basson C.T. *et al.* (1997) **Mutations in human TBX5 [corrected] cause limb and cardiac malformation in Holt-Oram syndrome** *Nat Genet* **15**:30–35

23. Li Q.Y. *et al.* (1997) **Holt-Oram syndrome is caused by mutations in TBX5, a member of the Brachyury (T) gene family** *Nat Genet* **15**:21–29

24. Basson C.T., Cowley G.S., Solomon S.D., Weissman B., Poznanski A.K., Traill T.A., Seidman J.G., Seidman C.E. (1994) **The clinical and genetic spectrum of the Holt-Oram syndrome (heart-hand syndrome)** *N Engl J Med* **330**:885–891

25. Hiroi Y., Kudoh S., Monzen K., Ikeda Y., Yazaki Y., Nagai R., Komuro I. (2001) **Tbx5 associates with Nkx2-5 and synergistically promotes cardiomyocyte differentiation** *Nat. Genet* **28**:276–280

26. Frank D.U., Carter K.L., Thomas K.R., Burr R.M., Bakker M.L., Coetzee W.A., Tristani-Firouzi M., Bamshad M.J., Christoffels V.M., Moon A.M. (2011) **Lethal arrhythmias in Tbx3-deficient mice reveal extreme dosage sensitivity of cardiac conduction system function and homeostasis** *PNAS* **109**:154–163

27. Meneghini V., Odent S., Platonova N., Egeo A., Merlo G.R. (2006) **Novel TBX3 mutation data in families with ulnar-mammary syndrome indicate a genotype-phenotype relationship: Mutations that do not disrupt the T-domain are associated with less severe limb defects** *Eur J Med Genet* **49**:151–158

28. Bamshad M. *et al.* (1997) **Mutations in human TBX3 alter limb, apocrine and genital development in ulnar-mammary syndrome** *Nat Genet* **16**:311–315

29. Linden H., Williams R., King J., Blair E., Kini U. (2009) **Ulnar Mammary syndrome and TBX3: expanding the phenotype** *Am. J. Med. Genet* **149**:2809–2812

30. Hoogaars W.M., Tessari A., Moorman A.F., de Boer P.A., Hagoort J., Soufan A.T., Campione M., Christoffels V.M. (2004) **The transcriptional repressor Tbx3 delineates the developing central conduction system of the heart** *Cardiovasc Res* **62**:489–499

31. Gurumurthy C.B. *et al.* (2021) **Response to correspondence on "Reproducibility of CRISPR-Cas9 methods for generation of conditional mouse alleles: a multi-center evaluation"** *Genome Biol* **22**

32. Dow L.E., Fisher J., O'Rourke K.P., Muley A., Kastenhuber E.R., Livshits G., Tschaharganeh D.F., Socci N.D., Lowe S.W. (2015) **Inducible in vivo genome editing with CRISPR-Cas9** *Nat Biotechnol* **33**:390–394

33. Pan X. *et al.* (2022) **Single-cell transcriptomics identifies Col1a1 and Col1a2 as hub genes in obesity-induced cardiac fibrosis** *Biochem Biophys Res Commun* **618**:30–37

34. Hua X., Wang Y., Jia P., Xiong Q., Hu Y., Chang Y., Lai S., Xu Y., Zhao Z., Song J. (2020) **Multi-level transcriptome sequencing identifies COL1A1 as a candidate marker in human heart failure progression** *BMC Med* **18**

35. Zhao J., Lv T., Quan J., Zhao W., Song J., Li Z., Lei H., Huang W., Ran L. (2018) **Identification of target genes in cardiomyopathy with fibrosis and cardiac remodeling** *J Biomed Sci* **25**

36. Ackerman J.E., Muscat S.N., Adjei-Sowah E., Korcari A., Nichols A.E.C., Buckley M.R., Loiselle A.E. (2024) **Identification of Periostin as a critical niche for myofibroblast dynamics and fibrosis during tendon healing** *Matrix Biol* **125**:59–72

37. Wu S. *et al.* (2024) **The gene expression of CALD1, CDH2, and POSTN in fibroblast are related to idiopathic pulmonary fibrosis** *Front Immunol* **15**

38. Oka T. *et al.* (2007) **Genetic Manipulation of Periostin Expression Reveals a Role in Cardiac Hypertrophy and Ventricular Remodeling** *Circ Res* **101**:313–321

39. van Eif V.W.W., Stefanovic S., Mohan R.A., Christoffels V.M. (2020) **Gradual differentiation and confinement of the cardiac conduction system as indicated by marker gene expression** *BBA - Molecular Cell Research* **867**

40. Verheule S., Kaese S. (2013) **Connexin diversity in the heart: insights from transgenic mouse models** *Front Pharmacol* **4**

41. Liang X., Wang G., Lin L., Lowe J., Zhang Q., Bu L., Chen Y., Chen J., Sun Y., Evans S.M. (2013) **HCN4 dynamically marks the first heart field and conduction system precursors** *Circ. Res* **113**:399–407

42. Greener I.D. *et al.* (2011) **Molecular architecture of the human specialized atrioventricular conduction axis** *J Mol Cell Cardiol* **50**:642–651

43. Mangoni M.E. *et al.* (2006) **Bradycardia and slowing of the atrioventricular conduction in mice lacking CaV3.1/alpha1G T-type calcium channels** *Circ. Res* **98**:1422–1430

44. Marionneau C., Couette B., Liu J., Li H., Mangoni M.E., Nargeot J., Lei M., Escande D., Demolombe S. (2005) **Specific pattern of ionic channel gene expression associated with pacemaker activity in the mouse heart** *J. Physiol* **562**:223–234

45. Garcia-Frigola C., Shi Y., Evans S.M. (2003) **Expression of the hyperpolarization-activated cyclic nucleotide-gated cation channel HCN4 during mouse heart development** *Gene Expr. Patterns* **3**:777–783

46. Schram G., Pourrier M., Melnyk P., Nattel S. (2002) **Differential distribution of cardiac ion channel expression as a basis for regional specialization in electrical function** *Circ Res* **90**:939–950

47. Donner B.C., Schullenberg M., Geduldig N., Hüning A., Mersmann J., Zacharowski K., Kovacevic A., Decking U., Aller M.I., Schmidt K.G. (2011) **Functional role of TASK-1 in the heart: studies in TASK-1-deficient mice show prolonged cardiac repolarization and reduced heart rate variability** *Basic Res Cardiol* **106**:75–87

48. Miquerol L., Moreno-Rascon N., Beyer S., Dupays L., Meilhac S.M., Buckingham M.E., Franco D., Kelly R.G. (2010) **Biphasic development of the mammalian ventricular conduction system** *Circ Res* **107**:153–161

49. Remme C.A. *et al.* (2009) **The cardiac sodium channel displays differential distribution in the conduction system and transmural heterogeneity in the murine ventricular myocardium** *Basic Res Cardiol* **104**:511–522

50. Graham V., Zhang H., Willis S., Creazzo T.L. (2006) **Expression of a two-pore domain K+ channel (TASK-1) in developing avian and mouse ventricular conduction systems** *Dev Dyn* **235**:143–151

51. Alcolea S., Theveniau-Ruissy M., Jarry-Guichard T., Marics I., Tzouanacou E., Chauvin J.P., Briand J.P., Moorman A.F.M., Lamers W.H., Gros D.B. (1999) **Downregulation of connexin 45 gene products during mouse heart development** *Circ. Res* **84**:1365–1379

52. van Kempen M.J.A., Vermeulen J.L.M., Moorman A.F.M., Gros D.B., Paul D.L., Lamers W.H. (1996) **Developmental changes of connexin40 and connexin43 mRNA distribution patterns in the rat heart** *Cardiovasc Res* **32**:886–900

53. Mohan R.A. *et al.* (2020) **T-box transcription factor 3 governs a transcriptional program for the function of the mouse atrioventricular conduction system** *Proc Natl Acad Sci U S A* **117**:18617–18626

54. van Eif V.W.W., Devalla H.D., Boink G.J.J., Christoffels V.M. (2018) **Transcriptional regulation of the cardiac conduction system** *Nat Rev Cardiol* **15**:617–630

55. Sander J.D., Maeder M.L., Reyon D., Voytas D.F., Joung J.K., Dobbs D. (2010) **ZiFiT (zinc finger targeter): an updated zinc finger engineering tool** *Nucleic Acids Research* **38**:W462–W468

56. Wheeler M.T., Allikian M.J., Heydemann A., Hadhazy M., Zarnegar S., McNally E.M. (2004) **Smooth muscle cell–extrinsic vascular spasm arises from cardiomyocyte degeneration in sarcoglycan-deficient cardiomyopathy** *JCI* **113**:668–675

57. Nadadur R.D. *et al.* (2016) **Pitx2 modulates a Tbx5-dependent gene regulatory network to maintain atrial rhythm** *Sci Transl Med* **8**

58. Liu F., Levin M.D., Petrenko N.B., Lu M.M., Wang T., Yuan L.J., Stout A.L., Epstein J.A., Patel V.V. (2008) **Histone-deacetylase inhibition reverses atrial arrhythmia inducibility and fibrosis in cardiac hypertrophy independent of angiotensin** *J Mol Cell Cardiol* **45**:715–723

59. Patel V.V., Arad M., Moskowitz I.P., Maguire C.T., Branco D., Seidman J.G., Seidman C.E., Berul C.I. (2003) **Electrophysiologic characterization and postnatal development of ventricular pre-excitation in a mouse model of cardiac hypertrophy and Wolff-Parkinson-White syndrome** *J Am Coll Cardiol* **42**:942–951

60. Gehrmann J., Berul C.I. (2000) **Cardiac electrophysiology in genetically engineered mice** *J Cardiovasc Electr* **11**:354–368

61. George S.A., Kiss A., Obaid S.N., Venegas A., Talapatra T., Wei C., Efimova T., Efimov I.R. (2020) **p38δ genetic ablation protects female mice from anthracycline cardiotoxicity** *Am J Physiol Heart Circ Physiol* **319**:H775–H786

62. Warhol A., George S.A., Obaid S.N., Efimova T., Efimov I.R. (2021) **Differential cardiotoxic electrocardiographic response to doxorubicin treatment in conscious versus anesthetized mice** *Physiol Rep* **9**

63. Cathey B., Obaid S., Zolotarev A.M., Pryamonosov R.A., Syunyaev R.A., George S.A., Efimov I.R. (2019) **Open-Source Multiparametric Optocardiography** *Sci Rep* **9**

64. Tamaddon H.S., Vaidya D., Simon A.M., Paul D.L., Jalife J., Morley G.E. (2000) **High-resolution optical mapping of the right bundle branch in connexin40 knockout mice reveals slow conduction in the specialized conduction system** *Circ Res* **87**:929–936

65. Laughner J.I., Ng F.S., Sulkin M.S., Arthur R.M., Efimov I.R. (2012) **Processing and analysis of cardiac optical mapping data obtained with potentiometric dyes** *Am J Physiol Heart Circ Physiol* **303**:H753–H765

66. Silverman M.E., Grove D., Upshaw C.B. (2006) **Why does the heart beat? The discovery of the electrical system of the heart** *Circulation* **113**:2775–2781

67. Masino A.M., Gallardo T.D, Wilcox C.A., Olson E.N., Williams R.S., Garry D.J. (2004) **Transcriptional regulation of cardiac progenitor cell populations** *Circ Res* **94**:389–397

68. Livak K.J., Schmittgen T.D. (2001) **Analysis of relative gene expression data using real-time quantitative PCR and the 2(-Delta Delta C(T)) method** *Methods* **25**:402–408

69. Rasband W.S. (2016) **ImageJ** Bethesda, MD, USA: U. S. National Institutes of Health

70. Wheeler M.T., Allikian M.J., Heydemann A., Hadhazy M., Zarnegar S., McNally E.M. (2004) **Smooth muscle cell-extrinsic vascular spasm arises from cardiomyocyte degeneration in sarcoglycan-deficient cardiomyopathy** *J Clin Invest* **113**:668–675

71. Benjamini Y., Hochberg Y. (1995) **Controlling the false discovery rate: a practical and powerful approach to multiple testing** *J Royal Stat Soc Ser B* **57**:289–300

72. Hoffmann A.D., Yang X.H., Burnicka-Turek O., Bosman J.D., Ren X., Steimle J.D., Vokes S.A., McMahon A.P., Kalinichenko V.V., Moskowitz I.P. (2014) **Foxf Genes Integrate Tbx5 and Hedgehog Pathways in the Second Heart Field for Cardiac Septation** *PLoS Genet* **10**

73. Xie L., Hoffmann A.D., Burnicka-Turek O., Friedland-Little J.M., Zhang K., Moskowitz I.P. (2012) **Tbx5-hedgehog molecular networks are essential in the second heart field for atrial septation** *Dev Cell* **23**:280–291

74. Verzi M.P., McCulley D.J., De Val S., Dodou E., Black B.L. (2005) **The right ventricle, outflow tract, and ventricular septum comprise a restricted expression domain within the secondary/anterior heart field** *Dev Biol* **287**:134–145

Author information

Ozanna Burnicka-Turek
Departments of Pediatrics, Pathology, and Human Genetics, University of Chicago, Chicago, USA
ORCID iD: 0000-0002-3770-4314

For correspondence: burnickatureko@uchicago.edu

Katy A Trampel
Departments of Biomedical Engineering, Northwestern University, Chicago, USA

Brigitte Laforest
Departments of Pediatrics, Pathology, and Human Genetics, University of Chicago, Chicago, USA
ORCID iD: 0000-0001-6919-8922

Michael T Broman
Department of Medicine, Section of Cardiology, University of Chicago, Chicago, USA

Zoheb Khan
Departments of Pediatrics, Pathology, and Human Genetics, University of Chicago, Chicago, USA

Eric Rytkin
Departments of Biomedical Engineering, Northwestern University, Chicago, USA

Binjie Li
Departments of Biomedical Engineering, Northwestern University, Chicago, USA

Ella Schaffer
Departments of Pediatrics, Pathology, and Human Genetics, University of Chicago, Chicago, USA

Margaret Gadek
Departments of Pediatrics, Pathology, and Human Genetics, University of Chicago, Chicago, USA

Kaitlyn M Shen
Departments of Pediatrics, Pathology, and Human Genetics, University of Chicago, Chicago, USA

Igor R Efimov
Departments of Biomedical Engineering, Northwestern University, Chicago, USA
ORCID iD: 0000-0002-1483-5039

Ivan P Moskowitz
Departments of Pediatrics, Pathology, and Human Genetics, University of Chicago, Chicago, USA

ORCID iD: 0000-0003-0014-4963

For correspondence: imoskowitz@uchicago.edu

Editors

Reviewer #1 (Public review):

Summary:

In a heroic effort, Ozanna Burnicka-Turek et al. have made and investigated conduction system-specific Tbx3-Tbx5 deficient mice and investigated their cardiac phenotype. Perhaps according to expectations, given the body of literature on the function of the two T-box transcription factors in the heart/conduction system, the cardiomyocytes of the ventricular conduction system seemed to convert to "ordinary" ventricular working myocytes. As a consequence, loss of VCS-specific conduction system propagation was observed in the compound KO mice, associated with PR and QRS prolongation and elevated susceptibility to ventricular tachycardia.

Strengths:

Great genetic model. Phenotypic consequences at the organ and organismal levels are well investigated. The requirement of both Tbx3 and Tbx5 for maintaining VCS cell state has been demonstrated.

Weaknesses:

The actual cell state of the Tbx3/Tbx5 deficient conducting cells was not investigated in detail, and therefore, these cells could well only partially convert to working cardiomyocytes, and may, in reality, acquire a unique state.

https://doi.org/10.7554/eLife.102027.1.sa2

Reviewer #2 (Public review):

Summary:

The goal of this work is to define the functions of T-box transcription factors Tbx3 and Tbx5 in the adult mouse ventricular cardiac conduction system (VCS) using a novel conditional mouse allele in which both genes are targeted in cis. A series of studies over the past 2 decades by this group and others have shown that Tbx3 is a transcriptional repressor that patterns the conduction system by repressing genes associated with working myocardium, while Tbx5 is a potent transcriptional activator of "fast" conduction system genes in the VCS. In a previous work, the authors of the present study further demonstrated that Tbx3 and Tbx5 exhibit an epistatic relationship whereby the relief of Tbx3-mediated repression through VCS conditional haploinsufficiency allows better toleration of Tbx5 VCS haploinsufficiency. Conversely, excess Tbx3-mediated repression through overexpression

results in disruption of the fast-conduction gene network despite normal levels of Tbx5. Based on these data the authors proposed a model in which repressive functions of Tbx3 drive the adoption of conduction system fate, followed by segregation into a fast-conducting VCS and slow-conduction AVN through modulation of the Tbx5/Tbx3 ratio in these respective tissue compartments.

The question motivating the present work is: If Tbx5/Tbx3 ratio is important for slow versus fast VCS identity, what happens when both genes are completely deleted from the VCS? Is conduction system identity completely lost without both factors and if so, does the VCS network transform into a working myocardium-like state? To address this question, the authors have generated a novel mouse line in which both Tbx5 and Tbx3 are floxed on the same allele, allowing complete conditional deletion of both factors using the VCS-specific MinK-CreERT2 line, convincingly validated in previous work. The goal is to use these double conditional knockout mice to further explore the model of Tbx3/Tbx5 co-dependent gene networks and VCS patterning. First, the authors demonstrate that the double conditional knockout allele results in the expected loss of Tbx3 and Tbx5 specifically in the VCS when crossed with Mink-CreERT2 and induced with tamoxifen. The double conditional knockout also results in premature mortality. Detailed electrophysiological phenotyping demonstrated prolonged PR and QRS intervals, inducible ventricular tachycardia, and evidence of abnormal impulse propagation along the septal aspect of the right ventricle. In addition, the mutants exhibit downregulation of VCS genes responsible for both fast conduction AND slow conduction phenotypes with upregulation of 2 working myocardial genes including connexin-43. The authors conclude that loss of both Tbx3 and Tbx5 results in "reversion" or "transformation" of the VCS network to a working myocardial phenotype, which they further claim is a prediction of their model and establishes that Tbx3 and Tbx5 "coordinate" transcriptional control of VCS identity.

Overall Appraisal:

As noted above, the present study does not further explore the Tbx5/Tbx3 ratio concept since both genes are completely knocked out in the VCS. Instead, the main claims are that the absence of both factors results in a transcriptional shift of conduction tissue towards a working myocardial phenotype, and that this shift indicates that Tbx5 and Tbx3 "coordinate" to control VCS identity and function. However, only limited data are presented to support the claim of transcriptional reprogramming since the knockout cells are not directly compared to working myocardial cells at the transcriptional level and only a small number of key genes are assessed (versus genome-wide assessment). In addition, the optical mapping dataset is incomplete and has alternative interpretations that are not excluded or thoroughly discussed.

In sum, while this study adds an elegantly constructed genetic model to the field, the data presented fit well within the existing paradigm of established functions of Tbx3 and Tbx5 in the VCS and in that sense do not decisively advance the field. Moreover, the authors' claims about the implications of the data are not always strongly supported by the data presented and do not fully explore alternative possibilities.

Strengths:

(1) Successful generation of a novel Tbx3-Tbx5 double conditional mouse model.

(2) Successful VCS-specific deletion of Tbx3 and Tbx5 using a VCS-specific inducible Cre driver line.

(3) Well-powered and convincing assessments of mortality and physiological phenotypes.

(4) Isolation of genetically modified VCS cells using flow.

Weaknesses:

(1) In general, the data is consistent with a long-standing and well-supported model in which Tbx3 represses working myocardial genes and Tbx5 activates the expression of VCS genes, which seem like distinct roles in VCS patterning. However, the authors move between different descriptions of the functional relationship and epistatic relationship between these factors, including terms like "cooperative", "coordinated", and "distinct" at various points. In a similar vein, sometimes terms like "reversion" are used to describe how VCS cells change after Tbx3/Tbx5 conditional knockout, and other times "transcriptional shift" and at other times "reprogramming". But these are all different concepts. The lack of a clear and consistent terminology for describing the phenomena observed makes the overarching claims of the manuscript more difficult to evaluate.

(2) A more direct quantitative comparison of Tbx5 Adult VCS KO with Tbx5/Tbx3 Adult VCS double KO would be helpful to ascertain whether deletion of Tbx3 on top of Tbx5 deletion changes the underlying phenotype in some discernable way beyond mRNA expression of a few genes. Superficially, the phenotypes look quite similar at the EKG and arrhythmia inducibility level and no optical mapping data from a single Tbx5 KO is presented for comparison to the double KO.

(3) The authors claim that double knockout VCS cells transform to working myocardial fate, but there is no comparison of gene expression levels between actual working myocardial cells and the Tbx3/Tbx5 DKO VCS cells so it's hard to know if the data reflect an actual cell state change or a more non-specific phenomenon with global dysregulation of gene expression or perhaps dedifferentiation. I understand that the upregulation of Gja1 and Smpx is intended to address this, but it's only two genes and it seems relevant to understand their degree of expression relative to actual working myocardium. In addition, the gene panel is somewhat limited and does not include other key transcriptional regulators in the VCS such as Irx3 and Nkx2-5. RNA-seq in these populations would provide a clearer comparison among the groups.

(4) From the optical mapping data, it is difficult to distinguish between the presence of (a) a focal proximal right bundle branch block due to dysregulation of gene expression in the VCS but overall preservation of the right bundle and its distal ramifications; from (b) actual loss of the VCS with reversion of VCS cells to a working myocardial fate. Related to this, the authors claim that this experiment allows for direct visualization of His bundle activation, but can the authors confirm or provide evidence that the tissue penetration of their imaging modality allows for imaging of a deep structure like the AV bundle as opposed to the right bundle branch which is more superficial? Does the timing of the separation of the sharp deflection from the subsequent local activation suggest visualization of more distal components of the VCS rather than the AV bundle itself? Additional clarification would be helpful.

Impact:

The present study contributes a novel and elegantly constructed mouse model to the field. The data presented generally corroborate existing models of transcriptional regulation in the VCS but do not, as presented, constitute a decisive advance.

https://doi.org/10.7554/eLife.102027.1.sa1

Reviewer #3 (Public review):

Summary:

In the study presented by Burnicka-Turek et al., the authors generated for the first time a mouse model to cause the combined conditional deletion of Tbx3 and Tbx5 genes. This has been impossible to achieve to date due to the proximity of these genes in chromosome 5,

preventing the generation of loss of function strategies to delete simultaneously both genes. It is known that both Tbx3 and Tbx5 are required for the development of the cardiac conduction system by transcription factor-specific but also overlapping roles as seen in the common and diverse cardiac defects found in patients with mutations for these genes. After validating the deletion efficiency and specificity of the line, the authors characterised the cardiac phenotype associated with the cardiac conduction system (CCS)-specific combined deletion of Tbx5 and Tbx3 in the adult by inducing the activation of the CCS-specific tamoxifen-inducible Cre recombination (MinK-creERT) at 6 weeks after birth. Their analysis of 8-9-week-old animals did not identify any major morphological cardiac defects. However, the authors found conduction defects including prolonged PR and QTR intervals and ventricular tachycardia causing the death of the double mutants, which do not survive more than 3 months after tamoxifen induction. Molecular and optical mapping analysis of the ventricular conduction system (VCS) of these mutants concluded that, in the absence of Tbx5 and Tbx3 function, the cells forming the ventricular conduction system (VCS) become working myocardium and lose the specific contractile features characterising VCS cells. Altogether, the study identified the critical combined role of Tbx3 and Tbx5 in the maintenance of the VCS in adulthood.

Strengths:

The study generated a new animal model to study the combined deletion of Tbx5 and Tbx3 in the cardiac conduction system. This unique model has provided the authors with the perfect tool to answer their biological questions. The study includes top-class methodologies to assess the functional defects present in the different mutants analysed, and gathered very robust functional data on the conduction defects present in these mutants. They also applied optical action potential (OAP) methods to demonstrate the loss of conduction action potential and the acquisition of working myocardium action potentials in the affected cells because of Tbx5/Tbx3 loss of function. The study used simpler molecular and morphological analysis to demonstrate that there are no major morphological defects in these mutants and that indeed, the conduction defects found are due to the acquisition of working myocardium features by the VCS cells. Altogether, this study identified the critical role of these transcription factors in the maintenance of the VCS in the adult heart.

Weaknesses:

In the opinion of this reviewer, the weakness in the study lies in the morphological and molecular characterization. The morphological analysis simply described the absence of general cardiac defects in the adult heart, however, whether the CCS tissues are present or not was not investigated. Lineage tracing analysis using the reporter lines included in the crosses described in the study will determine if there are changes in CCS tissue composition in the different mutants studied. Similarly, combining this reporter analysis with the molecular markers found to be dysregulated by qPCR and western blot, will demonstrate that indeed the cells that were specified as VCS in the adult heart, become working myocardium in the absence of Tbx3 and Tbx5 function.

https://doi.org/10.7554/eLife.102027.1.sa0

Author response:

> ***eLife Assessment***
>
> *"The work presented is important for our understanding of the development of the cardiac conduction system and its regulation by T-box transcription factors. The conclusions are supported by convincing data. Overall, this is an excellent study that*

> *advances our understanding of cardiac biology and has implications beyond the immediate field of study."*

We appreciate the positive assessment of this work and the recognition of its importance in advancing our understanding of the cardiac conduction system, its regulation by T-box transcription factors, and contribution beyond the immediate field.

> ***Reviewer #1 (Public review):***
>
> *Summary:*
>
> *In a heroic effort, Ozanna Burnicka-Turek et al. have made and investigated conduction system-specific Tbx3-Tbx5 deficient mice and investigated their cardiac phenotype. Perhaps according to expectations, given the body of literature on the function of the two T-box transcription factors in the heart/conduction system, the cardiomyocytes of the ventricular conduction system seemed to convert to "ordinary" ventricular working myocytes. As a consequence, loss of VCS-specific conduction system propagation was observed in the compound KO mice, associated with PR and QRS prolongation and elevated susceptibility to ventricular tachycardia.*
>
> *Strengths:*
>
> *Great genetic model. Phenotypic consequences at the organ and organismal levels are well investigated. The requirement of both* Tbx3 *and* Tbx5 *for maintaining VCS cell state has been demonstrated.*

We thank Reviewer #1 for acknowledging the effort involved in generating and characterizing the Tbx3/Tbx5 double conditional knockout mouse model and for highlighting the significance of this work in elucidating the role of these transcription factors in maintaining the functional and transcriptional identity of the ventricular conduction system.

> *Weaknesses:*
>
> *The actual cell state of the* Tbx3/Tbx5 *deficient conducting cells was not investigated in detail, and therefore, these cells could well only partially convert to working cardiomyocytes, and may, in reality, acquire a unique state.*

We agree with *Reviewer #1* that the *Tbx3/Tbx5* double mutant ventricular conduction myocardial cells may only partially convert to working cardiomyocytes or may acquire a unique state. The transcriptional state of the double mutant VCS cells was investigated by bulk profiling of key genes associated with specific conduction and non-conduction cardiac regions, including fast conduction, slow conduction, or working myocardium. Neither the bulk transcriptional approaches nor the optical mapping approaches we employed capture single-cell data; in both cases, the data represents aggregated signals from multiple cells (1, 2). Single cell approaches for transcriptional profiling and cellular electrophysiology would clarify this concern and are appropriate for future studies.

(1) O'Shea C, Nashitha Kabri S, Holmes AP, Lei M, Fabritz L, Rajpoot K, Pavlovic D (2020) Cardiac optical mapping – State-of-the-art and future challenges. *The International Journal of Biochemistry & Cell Biology* 126:105804. doi: 10.1016/j.biocel.2020.105804.

(2) Efimov IR, Nikolski VP, and Salama G (2004) Optical Imaging of the Heart. *Circulation Research* 95:21-33. doi: 10.1161/01.RES.0000130529.18016.35.

> ***Reviewer #2 (Public review):***
>
> *Summary:*

> *The goal of this work is to define the functions of T-box transcription factors* Tbx3 *and* Tbx5 *in the adult mouse ventricular cardiac conduction system (VCS) using a novel conditional mouse allele in which both genes are targeted in cis. A series of studies over the past 2 decades by this group and others have shown that* Tbx3 *is a transcriptional repressor that patterns the conduction system by repressing genes associated with working myocardium, while* Tbx5 *is a potent transcriptional activator of "fast" conduction system genes in the VCS. In a previous work, the authors of the present study further demonstrated that* Tbx3 *and* Tbx5 *exhibit an epistatic relationship whereby the relief of* Tbx3*-mediated repression through VCS conditional haploinsufficiency allows better toleration of* Tbx5 *VCS haploinsufficiency. Conversely, excess* Tbx3*-mediated repression through overexpression results in disruption of the fast-conduction gene network despite normal levels of* Tbx5*. Based on these data the authors proposed a model in which repressive functions of* Tbx3 *drive the adoption of conduction system fate, followed by segregation into a fast-conducting VCS and slow-conduction AVN through modulation of the* Tbx5/Tbx3 *ratio in these respective tissue compartments.*
>
> *The question motivating the present work is: If* Tbx5/Tbx3 *ratio is important for slow versus fast VCS identity, what happens when both genes are completely deleted from the VCS? Is conduction system identity completely lost without both factors and if so, does the VCS network transform into a working myocardium-like state? To address this question, the authors have generated a novel mouse line in which both* Tbx5 *and* Tbx3 *are floxed on the same allele, allowing complete conditional deletion of both factors using the VCS-specific* MinK-CreERT2 *line, convincingly validated in previous work. The goal is to use these double conditional knockout mice to further explore the model of* Tbx3/Tbx5 *co-dependent gene networks and VCS patterning. First, the authors demonstrate that the double conditional knockout allele results in the expected loss of* Tbx3 *and* Tbx5 *specifically in the VCS when crossed with* Mink-CreERT2 *and induced with tamoxifen. The double conditional knockout also results in premature mortality. Detailed electrophysiological phenotyping demonstrated prolonged PR and QRS intervals, inducible ventricular tachycardia, and evidence of abnormal impulse propagation along the septal aspect of the right ventricle. In addition, the mutants exhibit downregulation of VCS genes responsible for both fast conduction AND slow conduction phenotypes with upregulation of 2 working myocardial genes including connexin-43. The authors conclude that loss of both* Tbx3 *and* Tbx5 *results in "reversion" or "transformation" of the VCS network to a working myocardial phenotype, which they further claim is a prediction of their model and establishes that* Tbx3 *and* Tbx5 *"coordinate" transcriptional control of VCS identity.*

We appreciate Reviewer #2's detailed summary of the study's aims, methodologies, and findings, as well as their thoughtful suggestions for further analysis. We are grateful for their recognition of our genetic model's novelty and robustness.

> *Overall Appraisal:*
>
> *As noted above, the present study does not further explore the* Tbx5/Tbx3 *ratio concept since both genes are completely knocked out in the VCS. Instead, the main claims are that the absence of both factors results in a transcriptional shift of conduction tissue towards a working myocardial phenotype, and that this shift indicates that* Tbx5 *and* Tbx3 *"coordinate" to control VCS identity and function.*

We agree with this reviewer's assessment of the assertions in our manuscript. The novel combined *Tbx5/Tbx3* double mutant model does not further explore the TBX5/TBX3 ratio concept, which we previously examined in detail (1). Instead, as the Reviewer notes, this

manuscript focuses on testing a model that the coordinated activity of *Tbx3* and *Tbx5* defines specialized ventricular conduction identity.

(1) Burnicka-Turek O, Broman MT, Steimle JD, Boukens BJ, Petrenko NB, Ikegami K, Nadadur RD, Qiao Y, Arnolds DE, Yang XH, Patel VV, Nobrega MA, Efimov IR, Moskowitz IP (2020) Transcriptional Patterning of the Ventricular Cardiac Conduction System. *Circulation Research* 127:e94-e106. doi:10.1161/CIRCRESAHA.118.314460.

> *Strengths:*
>
> *(1) Successful generation of a novel* Tbx3-Tbx5 *double conditional mouse model.*
>
> *(2) Successful VCS-specific deletion of* Tbx3 *and* Tbx5 *using a VCS-specific inducible Cre driver line.*
>
> *(3) Well-powered and convincing assessments of mortality and physiological phenotypes.*
>
> *(4) Isolation of genetically modified VCS cells using flow.*

We thank Reviewer #2 for acknowledging the listed strengths of our study.

> *Weaknesses:*
>
> *(1) In general, the data is consistent with a long-standing and well-supported model in which* Tbx3 *represses working myocardial genes and* Tbx5 *activates the expression of VCS genes, which seem like distinct roles in VCS patterning. However, the authors move between different descriptions of the functional relationship and epistatic relationship between these factors, including terms like "cooperative", "coordinated", and "distinct" at various points. In a similar vein, sometimes terms like "reversion" are used to describe how VCS cells change after* Tbx3/Tbx5 *conditional knockout, and other times "transcriptional shift" and at other times "reprogramming". But these are all different concepts. The lack of a clear and consistent terminology for describing the phenomena observed makes the overarching claims of the manuscript more difficult to evaluate.*

We discriminate prior work on the “long-standing and well-supported model’ supported by investigation of the role of *Tbx5* and *Tbx3* independently from this work examining the coordinated role of *Tbx5* and *Tbx3*. Prior work demonstrated that *Tbx3* represses working myocardial genes and *Tbx5* activates expression of VCS genes, consistent with the reviewer’s suggestion of their distinct roles in VCS patterning. However, the current study uniquely evaluates the combined role of *Tbx3* and *Tbx5* in distinguishing specialized conduction identify from working myocardium, for the first time.

We appreciate Reviewer #2’s feedback regarding the need for consistent terminology when describing the impact of the double *Tbx3* and *Tbx5* mutant. We will edit the manuscript to replace terms like “reversion” with “transcriptional shift” or “transformation” when describing the observed phenotype, and we will use “coordination” to describe the combined role of *Tbx5* and *Tbx3* in maintaining VCS-specific identity.

> *(2) A more direct quantitative comparison of* Tbx5 *Adult VCS KO with* Tbx5/Tbx3 *Adult VCS double KO would be helpful to ascertain whether deletion of* Tbx3 *on top of* Tbx5 *deletion changes the underlying phenotype in some discernable way beyond mRNA expression of a few genes. Superficially, the phenotypes look quite similar at the EKG and arrhythmia inducibility level and no optical mapping data from a single* Tbx5 *KO is presented for comparison to the double KO.*

We thank Reviewer #2 for the suggestions that a direct comparison between *Tbx5* single conditional knockout and *Tbx3/Tbx5* double conditional knockout models may help isolate the specific contribution of *Tbx3* deletion in addition to *Tbx5* deletion.

Previous studies have assessed the effect of single *Tbx5* CKO in the VCS of murine hearts (1, 3, 5). Arnolds *et al.* demonstrated that the removal of *Tbx5* from the adult ventricular conduction system results in VCS slowing, including prolonged PR and QRS intervals, prolongation of the His duration and His-ventricular (HV) interval (3). Furthermore, Burnicka-Turek *et al.* demonstrated that the single conditional knockout of *Tbx5* in the adult VCS caused a shift toward a pacemaker cell state, with ectopic beats and inappropriate automaticity (1). Whole-cell patch clamping of VCS-specific *Tbx5*-deficient cells revealed action potentials characterized by a slower upstroke (phase 0), prolonged plateau (phase 2), delayed repolarization (phase 3), and enhanced phase 4 depolarization - features characteristic of nodal action potentials rather than typical VCS action potentials (3). These observations were interpreted as uncovering nodal potential of the VCS in the absence of *Tbx5*. Based on the role of Tbx3 in CCS specification (2), we hypothesized that the nodal state of the VCS uncovered in the absence of *Tbx5* was enabled by maintained *Tbx3* expression. This motivated us to generate the double *Tbx5 / Tbx3* knockout model to examine the state of the VCS in the absence of both T-box TFs.

In the current study, we demonstrate that the VCS-specific deletion of *Tbx3* and *Tbx5* results in the loss of fast electrical impulse propagation in the VCS, similar to that observed in the single *Tbx5* mutant. However, unlike the *Tbx5* single mutant, the *Tbx3/Tbx5* double deletion does not cause a gain of pacemaker cell state in the VCS. Instead, the physiological data suggests a transition toward non-conduction working myocardial physiology. This conclusion is supported by the presence of only a single upstroke in the optical action potential (OAP) recorded from the His bundle region and VCS cells in *Tbx3/Tbx5* double conditional knockout mice. The electrical properties of VCS cells in the double knockout are functionally indistinguishable from those of ventricular working myocardial cells. As a result, ventricular impulse propagation is significantly slowed, resembling activation through exogenous pacing rather than the rapid conduction typically associated with the VCS. We will edit the text of the manuscript to more carefully distinguish the observations between these models, as suggested.

(1) Burnicka-Turek O, Broman MT, Steimle JD, Boukens BJ, Petrenko NB, Ikegami K, Nadadur RD, Qiao Y, Arnolds DE, Yang XH, Patel VV, Nobrega MA, Efimov IR, Moskowitz IP (2020) Transcriptional Patterning of the Ventricular Cardiac Conduction System. *Circulation Research* 127:e94-e106. doi:10.1161/CIRCRESAHA.118.314460.

(2) Mohan RA, Bosada FM, van Weerd JH, van Duijvenboden K, Wang J, Mommersteeg MTM, Hooijkaas IB, Wakker V, de Gier-de Vries C, Coronel R, Boink GJJ, Bakkers J, Barnett P, Boukens BJ, Christoffels VM (2020) T-box transcription factor 3 governs a transcriptional program for the function of the mouse atrioventricular conduction system. *Proc Natl Acad Sci U S A.* 117:18617-18626. doi: 10.1073/pnas.1919379117.

(3) Arnolds DE, Liu F, Fahrenbach JP, Kim GH, Schillinger KJ, Smemo S, McNally EM, Nobrega MA, Patel VV, Moskowitz IP (2012) TBX5 drives Scn5a expression to regulate cardiac conduction system function. *The Journal of Clinical Investigation* 122:2509–2518. doi: 10.1172/JCI62617.

(4) Frank DU, Carter KL, Thomas KR, Burr RM, Bakker ML, Coetzee WA, Tristani-Firouzi M, Bamshad MJ, Christoffels VM, Moon AM (2012) Lethal arrhythmias in Tbx3-deficient mice reveal extreme dosage sensitivity of cardiac conduction system function and homeostasis. *Proc Natl Acad Sci U S A.* 109:E154-63. doi: 10.1073/pnas.1115165109.

(5) Moskowitz IP, Pizard A, Patel VV, Bruneau BG, Kim JB, Kupershmidt S, Roden D, Berul CI, Seidman CE, Seidman JG (2004) The T-Box transcription factor Tbx5 is required for the patterning and maturation of the murine cardiac conduction system. *Development 131*:4107-4116. doi: 10.1242/dev.01265. PMID: 15289437.

> *(3) The authors claim that double knockout VCS cells transform to working myocardial fate, but there is no comparison of gene expression levels between actual working myocardial cells and the* Tbx3/Tbx5 *DKO VCS cells so it's hard to know if the data reflect an actual cell state change or a more non-specific phenomenon with global dysregulation of gene expression or perhaps dedifferentiation. I understand that the upregulation of* Gja1 *and* Smpx *is intended to address this, but it's only two genes and it seems relevant to understand their degree of expression relative to actual working myocardium. In addition, the gene panel is somewhat limited and does not include other key transcriptional regulators in the VCS such as* Irx3 *and* Nkx2-5*. RNA-seq in these populations would provide a clearer comparison among the groups.*
>
> *And*
>
> *the main claims are that the absence of both factors results in a transcriptional shift of conduction tissue towards a working myocardial phenotype, and that this shift indicates that* Tbx5 *and* Tbx3 *"coordinate" to control VCS identity and function. However, only limited data are presented to support the claim of transcriptional reprogramming since the knockout cells are not directly compared to working myocardial cells at the transcriptional level and only a small number of key genes are assessed (versus genome-wide assessment).*

We appreciate Reviewer #2's suggestion to expand the gene expression analysis in *Tbx3/Tbx5*-deficient VCS cells by including other specific genes and comparisons with "native"/actual working ventricular myocardial cells and broadening the gene panel. In this study, we evaluated core cardiac conduction system markers, revealing a loss of conduction system-specific gene expression in the double mutant VCS. Furthermore, we evaluated key working myocardial markers normally excluded from the conduction system, *Gja1* and *Smpx*, revealing a shift towards a working myocardial state in the double mutant VCS (Figure 4). We agree that a more comprehensive analysis, such as transcriptome-wide approaches, would offer greater clarity on the extent and specificity of the observed shift from conduction to non-conduction identity. These approaches are appropriate directions for future studies.

> *(4) From the optical mapping data, it is difficult to distinguish between the presence of (a) a focal proximal right bundle branch block due to dysregulation of gene expression in the VCS but overall preservation of the right bundle and its distal ramifications; from (b) actual loss of the VCS with reversion of VCS cells to a working myocardial fate. Related to this, the authors claim that this experiment allows for direct visualization of His bundle activation, but can the authors confirm or provide evidence that the tissue penetration of their imaging modality allows for imaging of a deep structure like the AV bundle as opposed to the right bundle branch which is more superficial? Does the timing of the separation of the sharp deflection from the subsequent local activation suggest visualization of more distal components of the VCS rather than the AV bundle itself? Additional clarification would be helpful.*
>
> *And*
>
> *In addition, the optical mapping dataset is incomplete and has alternative interpretations that are not excluded or thoroughly discussed.*

We agree with Reviewer #2 that the resolution of the optical mapping experiment may be insufficient to precisely localize the conduction block due to the limited signal strength from the VCS. It is possible that the region defined as the His Bundle also includes portions of the right bundle branch. Our control mice show VCS OAP upstrokes consistent with those reported by Tamaddon *et al.* (2000) using Di-4-ANEPPS (1). We appreciate the Reviewer's attention to alternative interpretations, and we will incorporate these caveats into the manuscript text.

(1) Tamaddon HS, Vaidya D, Simon AM, Paul DL, Jalife J, Morley GE (2000) High-resolution optical mapping of the right bundle branch in connexin40 knockout mice reveals slow conduction in the specialized conduction system. *Circulation Research* 87:929-36. doi: 10.1161/01.res.87.10.929.

> *Impact:*
>
> *The present study contributes a novel and elegantly constructed mouse model to the field. The data presented generally corroborate existing models of transcriptional regulation in the VCS but do not, as presented, constitute a decisive advance.*
>
> *And*
>
> *In sum, while this study adds an elegantly constructed genetic model to the field, the data presented fit well within the existing paradigm of established functions of* Tbx3 *and* Tbx5 *in the VCS and in that sense do not decisively advance the field. Moreover, the authors' claims about the implications of the data are not always strongly supported by the data presented and do not fully explore alternative possibilities.*

We appreciate Reviewer # 2's acknowledgment of the elegance and novelty of the mouse model we generated. However, we respectfully disagree with their assessment that this work merely corroborates existing models without providing a decisive advance. Previous studies have investigated single *Tbx5* or *Tbx3* gene knockouts in-depth and established the T-box ratio model for distinguishing fast VCS from slow nodal conduction identity (1) that the reviewer alludes to in earlier comments. In contrast, this study aimed to explore a different model, that the combined effects of *Tbx5* and *Tbx3* distinguish adult VCS identity from non-conduction working myocardium. The coordinated *Tbx3* and *Tbx5* role in conduction system identify remained untested due to the lack of a mouse model that allowed their simultaneous removal. The very model the reviewer recognizes as "novel and elegantly constructed" has allowed the examination of the coordinated role of *Tbx5* and *Tbx3* for the first time. While we acknowledge the opportunity for additional depth of investigation of this model in future studies, the data we present provides consistent experimental support for the coordinated requirement of both *Tbx5* and *Tbx3* for ventricular cardiac conduction system identity.

(1) Burnicka-Turek O, Broman MT, Steimle JD, Boukens BJ, Petrenko NB, Ikegami K, Nadadur RD, Qiao Y, Arnolds DE, Yang XH, Patel VV, Nobrega MA, Efimov IR, Moskowitz IP (2020) Transcriptional Patterning of the Ventricular Cardiac Conduction System. *Circulation Research* 127:e94-e106. doi:10.1161/CIRCRESAHA.118.314460.

> ***Reviewer #3 (Public review):***
>
> *Summary:*
>
> *In the study presented by Burnicka-Turek* et al., *the authors generated for the first time a mouse model to cause the combined conditional deletion of* Tbx3 *and* Tbx5 *genes. This has been impossible to achieve to date due to the proximity of these genes in chromosome 5, preventing the generation of loss of function strategies to delete simultaneously both genes. It is known that both* Tbx3 *and* Tbx5 *are required for the*

> *development of the cardiac conduction system by transcription factor-specific but also overlapping roles as seen in the common and diverse cardiac defects found in patients with mutations for these genes. After validating the deletion efficiency and specificity of the line, the authors characterized the cardiac phenotype associated with the cardiac conduction system (CCS)-specific combined deletion of T_bx5_ and* Tbx3 *in the adult by inducing the activation of the CCS-specific tamoxifen-inducible Cre recombination (*MinK-creERT*) at 6 weeks after birth. Their analysis of 8-9-week-old animals did not identify any major morphological cardiac defects. However, the authors found conduction defects including prolonged PR and QTR intervals and ventricular tachycardia causing the death of the double mutants, which do not survive more than 3 months after tamoxifen induction. Molecular and optical mapping analysis of the ventricular conduction system (VCS) of these mutants concluded that, in the absence of* Tbx5 *and* Tbx3 *function, the cells forming the ventricular conduction system (VCS) become working myocardium and lose the specific contractile features characterizing VCS cells. Altogether, the study identified the critical combined role of* Tbx3 *and* Tbx5 *in the maintenance of the VCS in adulthood.*
>
> *Strengths:*
>
> *The study generated a new animal model to study the combined deletion of* Tbx5 *and* Tbx3 *in the cardiac conduction system. This unique model has provided the authors with the perfect tool to answer their biological questions. The study includes top-class methodologies to assess the functional defects present in the different mutants analyzed, and gathered very robust functional data on the conduction defects present in these mutants. They also applied optical action potential (OAP) methods to demonstrate the loss of conduction action potential and the acquisition of working myocardium action potentials in the affected cells because of* Tbx5/Tbx3 *loss of function. The study used simpler molecular and morphological analysis to demonstrate that there are no major morphological defects in these mutants and that indeed, the conduction defects found are due to the acquisition of working myocardium features by the VCS cells. Altogether, this study identified the critical role of these transcription factors in the maintenance of the VCS in the adult heart.*

We appreciate the Reviewer's comments regarding the originality and utility of our model and the strengths of our methodological approach. The Reviewer's appreciation of the molecular and morphological analyses as well as their constructive feedback is highly valuable.

> *Weaknesses:*
>
> *In the opinion of this reviewer, the weakness in the study lies in the morphological and molecular characterization. The morphological analysis simply described the absence of general cardiac defects in the adult heart, however, whether the CCS tissues are present or not was not investigated. Lineage tracing analysis using the reporter lines included in the crosses described in the study will determine if there are changes in CCS tissue composition in the different mutants studied. Similarly, combining this reporter analysis with the molecular markers found to be dysregulated by qPCR and western blot, will demonstrate that indeed the cells that were specified as VCS in the adult heart, become working myocardium in the absence of* Tbx3 *and* Tbx5 *function.*

We appreciate the reviewer's concern regarding the morphology of the cardiac conduction system in the *Tbx3/Tbx5* double conditional knockout model. We did not observe any structural abnormalities, as the Reviewer notes. We agree with their suggestion for using Genetic Inducible Fate Mapping to mark cardiac conduction cells expressing *MinKCre*. In fact, we utilized this approach to isolate VCS cells for transcriptional profiling. Specifically, we

combined the tamoxifen-inducible *MinKCreERT* allele with the Cre-dependent *R26Eyfp* reporter allele to label *MinKCre*-expressing cells in both control VCS and VCS-specific double *Tbx3*/*Tbx5* knockouts. EYFP-positive cells were isolated for transcriptional studies, ensuring that our analysis exclusively targeted conduction system-lineage marked cells. The ability to isolate *MinKCre*-marked cells from both controls and Tbx5/Tbx3 double mutants indicates that VCS cells persisted in the double knockout. Nonetheless, the suggestion for *in-vivo* marking by Genetic Inducible Fate Mapping and morphologic analysis is a valuable recommendation for future studies.

https://doi.org/10.7554/eLife.102027.1.sa4